3b2v7 AEA : 3662– Prod.Type:com pp.1–25(col.fig.:NIL) ED:Durai/Brr PAGN: chris SCAN: vinod

ARTICLE IN PRESS

PERGAMON

Atmospheric Environment ▮ (▮▮▮▮) ▮▮▮–▮▮▮

ATMOSPHERIC ENVIRONMENT

www.elsevier.com/locate/atmosenv

The MICS-Asia study: model intercomparison of long-range transport and sulfur deposition in East Asia

Gregory R. Carmichael[a,*], Giuseppe Calori[a], Hiroshi Hayami[b], Itsushi Uno[c], Seog Yeon Cho[a], Magnuz Engardt[d], Seung-Bum Kim[e], Yoichi Ichikawa[b], Yukoh Ikeda[f], Jung-Hun Woo[a], Hiromasa Ueda[g], Markus Amann[h]

[a] *Center for Global and Regional Environmental Research, University of Iowa, Iowa, USA*
[b] *Central Research Institute of Electric Power Industry, Komae, Japan*
[c] *Research Institute for Applied Mechanics, Kyushu University, Fukuoka, Japan*
[d] *Swedish Meteorological and Hydrological Institute, Sweden*
[e] *Department of Atmospheric Sciences, Yonsei University, Seoul, South Korea*
[f] *Osaka Prefecture University, Japan*
[g] *Disaster Prevention Research Center, Kyoto University, Kyoto, Japan*
[h] *International Institute for Applied Systems Analysis, Laxenburg, Austria*

Received 4 March 2001; accepted 26 August 2001

Abstract

An intercomparison study involving eight long-range transport models for sulfur deposition in East Asia has been initiated. The participating models included Eulerian and Lagrangian frameworks, with a wide variety of vertical resolutions and numerical approaches. Results from this study, in which models used common data sets for emissions, meteorology, and dry, wet and chemical conversion rates, are reported and discussed. Model results for sulfur dioxide and sulfate concentrations, wet deposition amounts, for the period January and May 1993, are compared with observed quantities at 18 surface sites in East Asia. At many sites the ensemble of models is found to have high skill in predicting observed quantities. At other sites all models show poor predictive capabilities. Source–receptor relationships estimated by the models are also compared. The models show a high degree of consistency in identifying the main source–receptor relationships, as well as in the relative contributions of wet/dry pathways for removal. But at some locations estimated deposition amounts can vary by a factor or 5. The influence of model structure and parameters on model performance is discussed. The main factors determining the deposition fields are the emissions and underlying meteorological fields. Model structure in terms of vertical resolution is found to be more important than the parameterizations used for chemical conversion and removal, as these processes are highly coupled and often work in compensating directions.

Keywords: Model intercomparision; Sulfur deposition; Long-range transport; Source–receptor relationships

1. Introduction

Fueled by high population growth and expanding economies, energy consumption in Asia is estimated to grow to 30% of the worlds total by 2015 (Shah et al., 2000). Since fossil fuels will continue to provide much of this energy, emissions of greenhouse gases and air pollutants such as sulfur and nitrogen oxides and particulates are projected to dramatically increase. The impacts of Asia's growth in emissions will have wide-ranging consequences (Streets et al., 1999). Acid precipitation is an illustrative example. China's National

*Corresponding author.
E-mail address: gcarmich@icaen.uiowa.edu (G.R. Carmichael).

1352-2310/01/$ - see front matter © 2001 Published by Elsevier Science Ltd.
PII: S1352-2310(01)00448-4

Environmental Protection Agency (NEPA) recently released a report indicating that economic losses due to acid rain damage to forests and farmland are five times higher than initially assessed in 1996, and are now estimated at $13.25 billion annually (Shah et al., 2000). The long-range transport and fate of pollutants in Asia is an area of increasing scientific interest and political concern, as countries receive growing amounts of pollutants from neighboring and even distant countries.

Long-range transport models play a critical role in science and policy analysis. These computer-based models calculate the distribution of trace gases in the troposphere and the quantities of acids deposited on the surface from specified emissions distributions and meteorological scenarios. The major features of such models consist of: (1) a transport component (or module) to describe the wind speed and direction, the eddy diffusivity and mixing layer height, the temperature, the water vapor, cloud water content, and the radiation intensity of each location as a function of time; (2) a chemical kinetic mechanism to describe the rates of atmospheric reactions, including homogeneous gas-phase, heterogeneous, and liquid-phase reactions; and (3) removal modules to describe the dry deposition of material, and the in-cloud and below-cloud removal processes. Each process incorporated into a model is itself a very complex and incompletely understood phenomenon. Therefore, in formulating such models it is necessary to incorporate the processes into the model framework by utilizing chemical, dynamic, and thermodynamic parameterizations. Furthermore, even processes that are well understood may require parameterization to maintain some balance of the details among the different processes that are treated in the model and the availability and quality of the supporting data needed to implement and evaluate the model components. In addition there are various approaches to modeling long-range transport (i.e., Lagrangian and Eulerian frameworks). Each model has its own strengths and weaknesses.

The potential for transboundary movement of sulfur and other pollutants means that domestic energy needs will become of increasing environmental concern (Shah et al., 2000; Guttikunda et al., 2001). Long-range transport models will be used to provide information on the transport and fate of emissions from various locations in East Asia. Source–receptor relationships in East Asia have been investigated by Arndt et al. (1998), Huang et al. (1995) and Ichikawa and Fujita (1995), Calori et al. (2001) and the results are very different. The calculated contribution of Chinese sources to Japan's deposition in these studies present markedly different estimates of the role that long-range transport plays in Japan's over-all deposition. Huang et al. (1995) estimated that China accounts for only 3.5% of Japan's total sulfur deposition. They found that over 93% of the sulfur deposited within Japan was from either Japanese anthropogenic or volcanic sources. In contrast, Ichikawa and Fujita (1995) estimated China to be a major source of wet sulfate deposition in Japan, accounting for one-half of the anthropogenic deposition. These variations are due in part to differences in removal rates and chemical conversion rates in different models. Low removal rates result in greater transport away from source locations and thus higher transboundary pollution. There is a great need to conduct model intercomparision studies to better understand how to model long-range transport in East Asia.

Previous work on intercomparing acid deposition models applied to Japan has been conducted. These include a joint study comparing CRIEPI (Central Research Institute of Electric Power Industry; Ichikawa and Fujita, 1995) and ATMOS (Arndt and Carmichael, 1995) trajectory models with Eulerian results (i.e., the STEM model, Carmichael et al., 1991). These results have been reported by Phadnis and Carmichael (1998).

A Workshop on the Transport of Air Pollutants in Asia was held at International Institute for Applied System Analysis (IIASA) in Laxenburg, Austria during 27–29 July 1998 (IIASA, 1998), and issues related to the modeling of long-range transport in Asia were discussed. The attendees recognized that in order to help improve the use of models in science and policy analyses in Asia it is necessary to have a better understanding of model performance and uncertainties. The group initiated a model intercomparison exercise to be performed as part of joint collaborative studies involving the CRIEPI/IIASA and the Regional Air Pollution INformation and Simulation (RAINS)-Asia projects. The results from this study are presented in this paper.

2. Intercomparison framework

2.1. Task subdivision and conditions

The study domain (Fig. 1) 95–150°E and 5–50°N, includes Southeast Asia, Philippines, Taiwan, Japan, North and South Korea, most of China, and parts of Russia and Mongolia. Two month-long periods were selected (January and May 1993), to reflect long-range transport conditions under two distinct seasons. During these periods measurements of sulfur concentrations and deposition were made throughout the study region using identical sampling and analysis protocols. A common meteorological data set was also prepared, using Regional Atmospheric Modeling System (RAMS) model, and provided to all participants.

The SO_2 emissions, based on the RAINS-Asia analyses, were supplied to participants through a web site (CGRER, 1999). They included emissions from area sources and large point sources, emissions from shipping activities and from volcanoes. Release heights were also specified: area emissions were to be injected in the first model layer; while large point sources and volcanoes were assigned effective release heights of 300 and 1500 m, respectively. Emissions were considered as 95% SO_2 and 5% SO_4.

Eulerian models were run with zero initial and boundary conditions for sulfur and were initialized for 48 h. Prescribed deposition velocities were also used, as specified in Table 1 and the related land/sea mask was also made available.

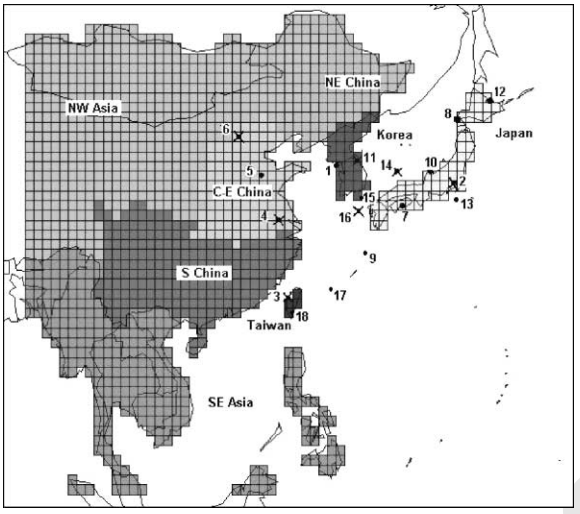

Fig. 1. Modeling domain with countries/regions sets for source–receptor calculations, measurement site locations (●) and receptor locations (×): (1) Kangwha; (2) Komae; (3) Taichung; (4) Nanjing; (5) Jinan; (6) Beijing; (7) Nangoku; (8) Otobe; (9) Amami; (10) Kashima; (11) Yangyang; (12) Tokoro; (13) Hachijo; (14) Oki; (15) Tsushima; (16) Fukue; (17) Miyako; (18) Taitong.

Table 1
Prescribed deposition velocities[a]

Species	Conditions	v_d (cm s^{-1})
SO_2	Land (April–September)	0.25
	Land (otherwise)	0.125
	Sea	0.32
SO_4	Land	0.2
	Sea	0.1

[a]These parameters were selected as a result of a review of current literatures. Details can be found in Guttikunda et al. (2001) and Calori et al. (2001).

2.1.1. Intercomparison tasks

The intercomparison activity consisted of four tasks. All participants were asked to do Task A, and as many of the other tasks as possible.

2.1.1.1. Task A—the blind test. Modelers were requested to use their models and the above information on emissions, meteorology, and dry deposition velocities, and calculate surface SO_2 and sulfate concentrations and sulfur deposition. They were allowed to use their best estimate of model parameters associated with chemical conversion and wet removal. Their results were reported for specific measurement site locations (Fig. 1) in terms of daily average concentrations and depositions. These data were compared to measurement values centrally by the study coordinators. Concentrations as well as wet and dry deposition fields at given times were also reported (see below for details).

Every model result was blind (i.e., only the organizers and the owner of the model knew their code number) and all results were reported using the code numbers. In addition each modeler submitted detailed information regarding model parameters.

2.1.1.2. Task B—the fixed parameter test. Extension of Task A, but modelers were given specific parameter values (Table 2) to use for SO_2 to sulfate conversion and wet removal of SO_2 and sulfate. Submitted results were the same as before.

2.1.1.3. Task C—the source–receptor test. Modelers submitted source–receptor information for a few prescribed receptor locations, selected from the measurement sites: Komae, Oki, Fukue, Yangyang, Beijing, Nanjing, Taichung. Contributions from various sets of

Table 2
Prescribed parameters for Task B[a]

Parameter	Value
$SO_2 \rightarrow SO_4$ conversion rate (s^{-1})	$K_0 f(\lambda) + K_1[1 - f(\lambda)]\, g(J)$
	where $K_0 = 1 \times 10^{-5}$ $K_1 = 4 \times 10^{-6}$ $f(\lambda) = \cos[1.3\lambda\pi/180]$ $g(J) = \sin[(J - 80)2\pi/365]$
SO_2 wet removal rate constant (s^{-1})	$2 \times 10^{-5} P$
SO_4 wet removal rate constant (s^{-1})	$5 \times 10^{-5} P^{0.83}$

[a]These parameters were selected as a result of a review of current literatures. Details can be found in Guttikunda et al. (2001) and Calori et al. (2001).

λ is latitude (°N), J is the Julian day and P is the precipitation rate (mm h^{-1}).

countries/regions (Fig. 1) and volcanic sources were requested.

2.1.1.4. Task D—the tuning test. Modelers were given the observation data and given the chance to rerun their model (changing parameters as they saw fit) and submit new results.

2.1.2. Model results reporting procedures

Reporting activities followed five stages, according to the task subdivisions. At each stage of the intercomparison participants were requested to submit data as well as relevant information to help in the interpretation of model results. The reporting procedures are outlined in Table 3. A code number was assigned to each registered participants, and was used when submitting model results.

2.2. Meteorological data

The study region has dramatic variation of topography, land type, and mixtures of industrial/urban centers and agricultural/rural regions. It also includes a large portion of ocean (more than 30% of the domain), where there is a void of in situ meteorological data and so the use of numerical models is crucial to capture the interactions between continental and marine air masses determining pollutants transport, transformation and deposition in the region. A common meteorological data set was prepared by Prof. Uno of Kyushu University (Uno and Jang, 1999) using the RAMS model (Pielke et al., 1992). RAMS includes the Kuo-type cumulus parameterization to represent the sub-grid scale convective cumulus and the Kessler-type microphysics model, able to simulate mesoscale cloud and precipitation phenomena. The surface flux calculation module in RAMS (Louis, 1979) was improved based on the result of Uno et al. (1995). The employed computational grid consists of 60×56 grid cells of 100 km each in horizontal, and 30 vertical levels following the topography, with the top level set as 23 km. Model field initialization and four-dimensional data assimilation (FDDA) were performed using a Newtonian relaxation ('nudging') based on the time-dependent lateral boundary conditions provided based on the European Centre for Medium-Range Weather Forecasts (ECMWF) 2.5° global analysis data. The initialization was performed 3 days before each monthly period and the nudging was prescribed every 12 h for 5 lateral grids.

At the ground surface, topography and the land/sea mask were obtained from the RAMS built-in data set, and the vegetation index was converted from Matthews data. (Matthews, 1983) Sea surface temperatures (SST) were taken from (National Center for Environmental Prediction (NCEP), US) database (Vazquez et al., 1998, $1^\circ \times 1^\circ$ resolution), while snow cover fraction was taken from International Satellite Land Surface Climatology Project (ISLSCP) Initiative I data set (Sellers et al., 1995; weekly data in 1987). The stored meteorological variables (every 3 h) distributed to the modelers included three-dimensional fields of wind components, air temperature, atmospheric pressure, water vapor mixing ratio, cloud water and rainwater, and 2D fields of surface temperature, friction velocity and temperature, precipitation rate.

2.2.1. General meteorological conditions

Fig. 2 shows the main meteorological features of the two simulated months. Winter monsoon (WM) is the weather type mostly characterizing the month of January, typically associated with high wind speed determining transboundary pollutant transport eastward of mainland Asia. Meteorological fields calculated by RAMS for January 1993 indicate the occurrence of transition weather types before the establishment of the WM. A Japan Sea low type (JSL) is observed from 2 to 4 January, while the CRIEPI observation period (11–21 January) is characterized by a sequence of different weather types: a typical winter monsoon type (WM, 11 January), followed by a South Coast low type (SCL, 12–16 January), a WM (16–20 January) and then again a SCL (23–26 January).

In May, the typical weather is characterized by the large scale traveling high pressure system moving very slowly eastward. However, in May 1993 such a system did not occur; rather only a small high speed traveling high pressure system was observed (i.e., 4–5, 16–17 May), with an intermediate west-east meso-front on 9–10 May.

The comparison between calculated and observed precipitation at monitoring sites on a monthly basis is presented in Fig. 3.

2.3. Observational data

Observational data used in this study were those obtained at the 18 stations (shown in Fig. 1) comprising the cooperative monitoring network for acid deposition in East Asia. The network was operated by the Institute of Water Conservancy and Hydroelectric Power Research (IWHR) in mainland China, Kon-Kuk University (KKU) in Korea, Taiwan Power Company in Taiwan, and the Central Research Institute of Electric Power Industry in Japan, for 3 years from October 1990. A major purpose of the monitoring was to build a data set of acid deposition for long-term, regional-scale evaluation in East Asia. The stations were carefully selected considering factors like climatic precipitation amounts, geology, source location, and convenience of maintenance, based on Robertson and Wilson (1985). See Fujita and Takahashi (1994) and Fujita et al. (2000) for more details.

Table 3
Outline of reporting procedures

Stage	Activities
Registration	All the groups participating to the intercomparison exercise were encouraged to register via e-mail, and to provide the following information: ● participant information (name, organization, planned contributions) ● model structure and purpose: model name, main model focus, modelled quantities, model type and dimension
Task A The blind test	**Data requested** ● *monitoring sites data set*: daily averaged surface concentrations of SO_2 and SO_4 and daily dry and wet sulfur ($SO_2 + SO_4$) depositions at the specified measurement site locations (see Fig. 1) ● *daily averaged surface concentrations fields*: 2D fields of daily averaged concentrations of SO_2 and SO_4 at the surface on every 10th day (i.e., 10 January, 20 January, 30 January, 10 May, … etc.) ● *daily averaged boundary layer concentrations fields*: 2D fields of daily averaged concentrations of SO_2 and SO_4, averaged from the ground to 1 km height on every 10th day (data set not required if identical to the one of daily averaged surface concentrations) ● *hourly averaged surface concentrations fields*: 2D fields of hourly averaged concentrations of SO_2 and SO_4 at 00 UTC hour on every 10 day ● *10 days averaged surface concentrations fields*: 2D fields of 10 days averaged concentrations of SO_2 and SO_4 at 00 UTC hour on every 10th day ● *10 days accumulated dry and wet depositions fields*: 2D fields of 10 days accumulated SO_2 and sulfate dry and wet depositions (i.e. 1–10 January, 11–20 January …) **Accompanying information** A description of model characteristics and modeling conditions: ● *model domain*: horizontal and vertical size and location of the domain, horizontal and vertical coordinates and grid system ● *physical and chemical processes*: basic assumptions, numerical schemes and adopted parameters for each process: transport and diffusion, chemistry, dry deposition, wet removal ● input data used: ○ topography ○ emissions: species list, spatial resolution, time frequency, sources types (area/point) ○ meteorology: source (e.g. observations vs. model), spatial resolution, time frequency, variables list ○ initial and boundary conditions: source (e.g. observations, other models…), type (e.g. fixed, variable in time…) ● *emissions summary* (if an emission data set different from the one made available for the intercomparison, a table with total emissions by country) ● *references*: all relevant references (preferably in open literature), pertaining to model formulation and previous applications
Task B The fixed parameter test	**Data requested** Same data sets as for Task A **Accompanying information** A detailed description of any parameterizations used in the model different from those prescribed
Task C The source–receptor test	**Data requested** *source–receptor relations*: contributions to total depositions from sets of countries/regions (Fig. 1) and volcanic sources at the prescribed receptor locations: Komae, Oki, Fukue, Yangyang, Beijing, Nanjing, Taichung
Task D The tuning test	Monitoring data have been provided to each participant after submission of model results for Tasks A, B and C **Data requested** Same data sets as for Task A **Accompanying information** adopted parameters for each of the following processes: chemical mechanism, dry deposition, wet removal

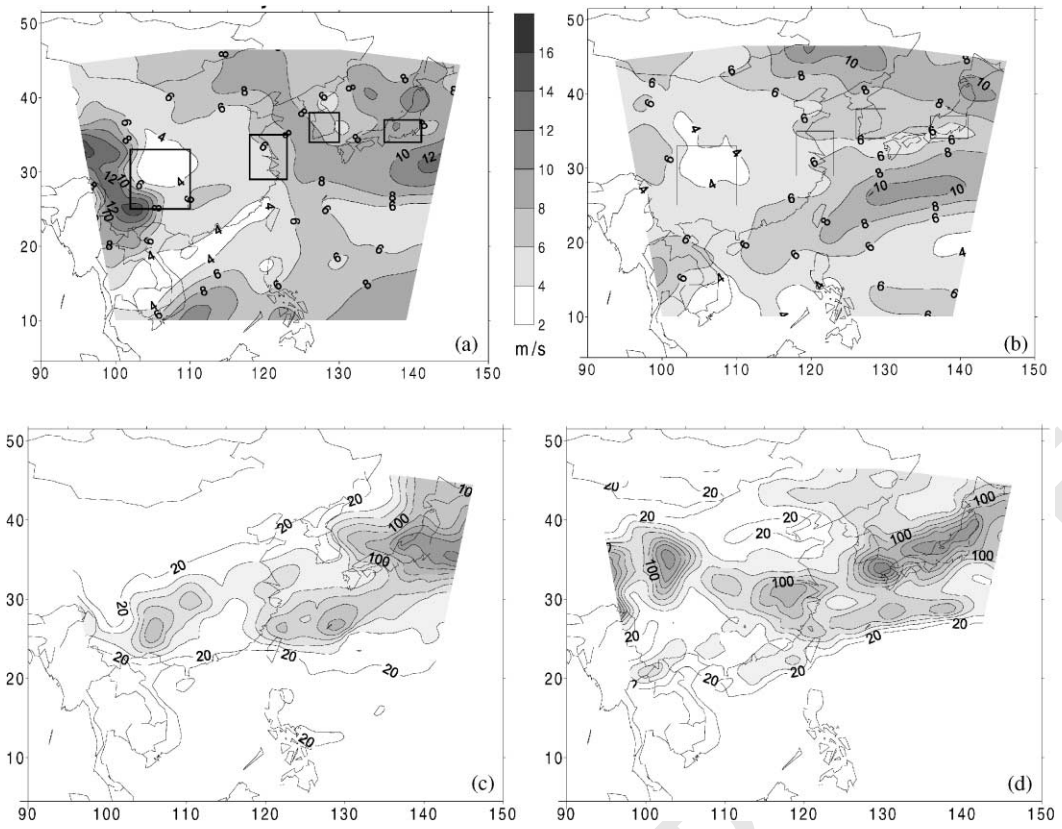

Fig. 2. Upper panels: monthly mean modeled winds at 1000 m sigma level: (a) January; (b) May; lower panels: monthly modeled total precipitation (mm): (c) January; (d) May.

Precipitation samples were collected with wet-only samplers with an aperture area of 190 cm^2. The top of the sampler was at approximately 150 cm above the ground level. The precipitation sensor of the sampler responded to rain drops with a diameter larger than 0.5 mm. Heaters were thermostatically controlled to prevent freezing and snow accumulation, when temperatures fell below 0°C. The amount of precipitation was measured using tipping-bucket rain gauges with a detection limit of 0.5 mm. Precipitation samples obtained at stations in China, Korea, Taiwan and Japan were transported to chemical laboratories of IWHR, KKU, National Taiwan University, and CRIEPI, respectively. Each laboratory used its own analytical method. The analytical parameters included pH, conductivity, Na^+, K^+, Ca^{2+}, Mg^{2+}, NH_4^+, SO_4^{2-}, NO_3^-, and Cl^-. Since there was no standard solution for chemical analysis of precipitation over East Asia, identical precipitation samples collected in Japan were sent to each laboratory to verify the analytical procedures. For conductivity and pH measurement, samples were analyzed without pretreatment. For other parameters, each sample was filtered through a Milipore filter with a pore size of 0.45 μm before analysis. The accuracy of chemical analysis was confirmed using two indices, the ratio of total anion to total cation and the ratio of measured to calculated conductivity, based on the method proposed by Miles and Yost (1982). Samples satisfying the condition that deviations of both index values were within ±0.2 were identified as 'valid samples'. This checking method was not always implemented for samples obtained in northern China, where relatively high pH values were observed.

Particle and SO_2 were collected using low-volume samplers with two-stage 47 mm diameter filter packs. The top of the sampler was at approximately 150 cm above the ground level. A Teflon filter was mounted on the upper stage to collect particles, and an alkaline filter on the lower stage to collect SO_2. The flow rate was set to match the gravitational settlement velocity for a 10 μm spherical particle with a density of 1 g cm^{-3} in the samplers. The alkaline filters were quartz filters impregnated with 6% K_2CO_3 solution for 2 h, which were prepared at CRIEPI and mailed to all the stations. The filters were extracted with ultrasonic

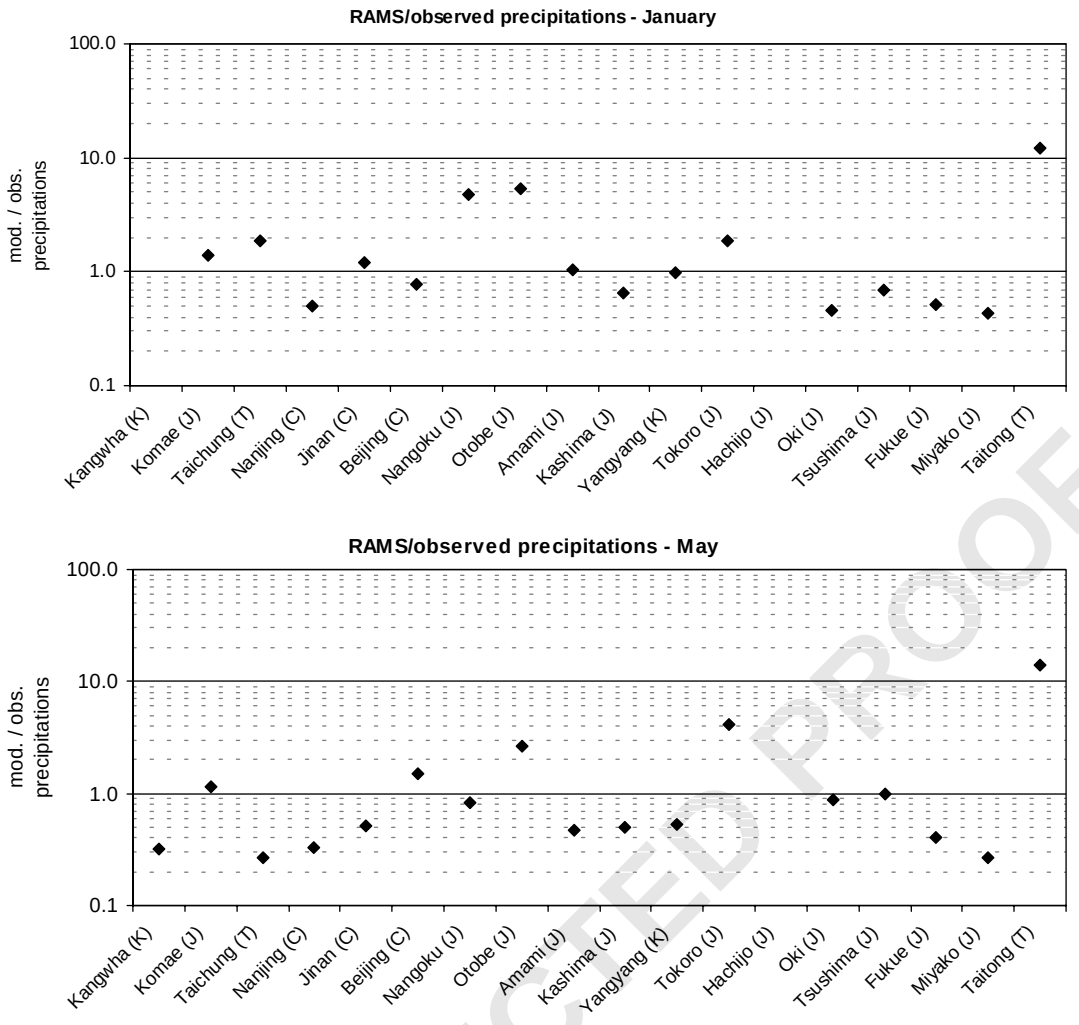

Fig. 3. Ratios between monthly calculated (RAMS) and observed precipitation at monitoring sites.

vibration for 1 h in approximately 20 ml of distilled water. The extracted solution was filtered using a Millipore filter and diluted to 50 ml. These filtered samples were analyzed with the same method as precipitation samples.

Two 10-day periods (one in each month) were selected for use in the intensive intercomparison excercises.

3. Participating models

The modeling community was informed of this intercomparison exercise in various ways. The study was announced at various technical meetings, including the 6th Atmospheric Sciences and Application to Air Quality (ASAAQ) Meeting in Beijing (November 1998), and RAINS-Asia Phase II Workshops in Beijing (November 1998) and Bangkok (May 1999). Announcements were also sent to the list of participants at these meetings and the CRIEPI/IIASA Workshop on Transport of Air Pollutants in Asia (Laxenburg, July 1998). After the announcement, CDs containing the necessary input data sets were sent to those responding.

Modeling groups that have submitted results to date are listed in Table 4, together with the main characteristics of their models and the contributions to the proposed tasks. Models differ substantially from each other, including the computational framework adopted (Eulerian or Lagrangian), the number of vertical layers and transport-diffusion algorithm used. These features are summarized in Tables 5 and 6. Chemical conversion and wet removal parameters adopted by models contributing to the "Blind test" (Task A) are also listed in Table 7. As for the chemical species, all models

Table 4
Groups and models participating to the model intercomparison

Participant(s)	Organization	Contribs.	Model name	Model type	Main model focus	References
S.-B. Kim, T.-Y. Lee, K.-Y. Ma	Department of Atmospheric Sciences, Yonsei University, Seoul (Korea)	A, B, C	YU-SADM (Yonsei University—Sulfur Acid Deposition Model)	3D Eulerian	Long-term period or episodic estimation of sulfur sources contributions	
H. Hayami, Y. Ichikawa	CRIEPI (Japan)	A, B, C	CRIEPI Trajectory Model	Lagrangian 1-layer	Long-term evaluation	Ichikawa and Fujita (1995)
H. Hayami, O. Hertel, Y. Ichikawa	CRIEPI (Japan) and National Environmental Research Institute (Denmark)	A, B, C	ACDEP ASIA	Lagrangian 1-layer	Long-term evaluation	
I. Uno, E.S. Jang	Research Institute for Applied Mechanics, Kyushu University, Fukuoka (Japan)	A[a], B, C	RIAM Version of RAMS On-Line Tracer Model	3D Eulerian	Episodic and long-term simulation for chemical climate studies	
Y. Ikeda, R. Yasuda, H. Nakaminami	Osaka Prefecture University (Japan)	A, B, C	OPU-Model (Osaka Prefecture University Model)	3D Eulerian	Long-term deposition	
S.Y. Cho, G. Carmichael	CGRER, University of Iowa	A[a], B, C	STEM	3D Eulerian	Episodic and long-term studies	Carmichael et al. (1991)
G. Calori, G. Carmichael	CGRER, University of Iowa	A[a], B, C	ATMOS-2	Lagrangian multi-layer	Long-term concentrations and depositions of sulfur in Asia. Source-receptor relationships.	Arndt and Carmichael (1995)
M. Engardt	Swedish Meteorological and Hydrological Institute	A, B	MATCH	3D Eulerian	Long-term concentrations and depositions of ozone and acidifying substances	Robertson et al. (1999)

[a] RIAM-RAMS, STEM, and ATMOS-2 used the same for Tasks A and B.

Table 5
Further specifics of 3D Eulerian models participating to the intercomparison

Model name	Vert. coord. system	Layers	Lowest layer (m)	Horizontal algorithm	K_h	Vertical algorithm	K_v
YU-SADM	σ_z	20 layers, up to 13 km (6 layers in ~1 km)	~50	Bott's 2nd order Bott (1989, 1992)	Neglected	Bott's 2nd order	profile method Brost et al., 1988)
RAMS/RIAM	σ_z	20 layers, up to 13 km (6 layers in ~1 km)	~50	RAMS	RAMS	RAMS	RAMS
OPU-Model	σ_z	7 layers, up to 5 km	100	Smolarkiewicz (1983)	Neglected	Crank–Nicholson	daytime/nighttime and layer-specific look-up table
STEM	σ_z	20 layers, up to 13 km (6 layers in ~1 km)	~50	Galerkin with upwinding	Neglected	Galerkin	RAMS
MATCH	Hybrid σ_p (ECMWF)	31 layers (5 layers in ~1 km)	~70	Bott's 2nd order Bott (1989, 1992)	Neglected	Bott's high-order	profile method

generally simulate sulfur dioxide and particulate sulfate, linked by a linear transformation and with both removed via dry and wet deposition pathways. A few exceptions exist. The OPU-Model, CRIEPI trajectory and ACDEP-ASIA models treat also sulfate in cloud water as a third transported species. The in-cloud scavenging process is then assumed to take place whether clouds exist or not (clouds are assumed to exist anytime, anywhere), to account for aqueous-phase production of SO_4 in non-precipitating clouds. A corresponding wet removal rate for cloud water sulfate adds a third removal pathway controlled by precipitation. All models used the meteorological data previously described, except MATCH, that used 6-hourly ECMWF data on a lat–lon grid at 1° resolution and 31 hybrid levels in the vertical.

4. Results

4.1. Comparison with observations

The initial analysis of the model predictions relative to the observations focused on results from Task A. Sample SO_2 concentration distributions calculated by participating models are shown in Fig. 4 (please note that Model 3 is a receptor oriented model, and did not produce 2D fields). Although absolute values differ from model to model, in all cases the surface SO_2 concentrations follow closely the emission distribution. The model predicted values are presented along with the observations in Figs. 5 and 6 for the 10 day events in January and May. In general the observations fall within the ensemble of the model predictions, with the exception being sulfur-wet deposition at sites like Taichung (which will be discussed later). Furthermore, all the models resolve the observed increase in sulfur deposition (by about one order of magnitude) over east China compared to Japan. The variability of the model predictions is largest over China, and is the smallest for the SO_2 predictions and largest for predictions of sulfur deposition (see Fig. 7 for the bias of model calculated quantities for the month of January). In general the models systematically under-predicted sulfate concentrations and wet sulfur deposition, and over-predicted SO_2 concentrations. This suggests an underestimation of the SO_2 to sulfate conversion rate and will be discussed in further detail in Sections 4.3 and 4.4.

The capability of the model ensemble of reproducing the observed values also varies site by site (see Fig. 8). For many locations the ensemble of models has appreciable skill in predicting sulfur deposition. However at a few sites, e.g., Oki, all models perform poorly. Possible reasons include uncertainties in regional/local emissions and transport pathways. However, similar

Table 6
Further specifics of Lagrangian models participating to the intercomparison

Model name	Layers	Trajectories type	Horizontal diffusion	Vertical diffusion
CRIEPI Traj. Model	1 layer: BL (1000 m)	backward (forward Euler procedure) on isobaric winds at 850 hPa or at the bottom σ_z, when surface pressure of the travelling air mass is below 850 hPa	Gaussian	uniform within the BL
ACDEP ASIA	1 layer: BL (variable height)	backward (Petterssen's procedure) on isosigma winds at $\sigma_z = 1000$ m	Gaussian, with $\sigma_h = 0.1d$ (m) d = travel distance (m)	uniform within the BL
ATMOS-2	2 or 3 layers: BL (variable height), free troposphere (6000 m), nighttime surface layer (300 m)	forward (iterative forward Euler procedure) on layer-averaged winds	Gaussian, with $\sigma_h = 0.5t$ (m) t = travel time (s)	uniform within each layer; mass exchanges among layers at sunrise and sunset

Table 7
Models-specific parameters for Task A[a]

Model code	$SO_2 \rightarrow SO_4$ conversion rate (s^{-1})	SO_2 wet removal rate (s^{-1})	SO_4 wet removal rate (s^{-1})
1	$k_c = \bar{k}[1 - 0.4\cos(2\pi H/24)]$ $\bar{k} = k_{EQ} + \frac{\lvert\lambda\rvert}{90}(k_{\mathrm{POLE}} - k_{EQ})$ $k_{EQ} = 4.0 \times 10^{-6}$ $k_{\mathrm{POLE}} = 1.3 \times 10^{-6} + 1.1 \times 10^{-6} \sin\gamma$ $\gamma = \begin{cases} \frac{2\pi(J+91)}{365}, & \lambda < 0 \\ \frac{2\pi(J-91)}{365}, & \lambda \geqslant 0 \end{cases}$ H = local time, J = Julian day, λ = latitude (Tarrasón, 1995)	$4 \times 10^{-5} P$	$10 \times 10^{-5} P$
2	$k_c = 0.3\times10^{-6} + 4.7\times10^{-6} \max\left(0; \frac{\sin(\theta(\lambda, J))}{\sin(\theta(50^\circ\mathrm{N}, 23\ \mathrm{June}))}\right)$ θ = height of the sun at midday, λ = latitude, J = Julian day (Christensen 1995)	$2 \times 10^{-5} P$	$2 \times 10^{-4} P^{0.7}$ (Maeda, 1998)
3 and 4	2.8×10^{-6} in January 8.5×10^{-5} in May 5.6×10^{-6} rainout	$2.8 \times 10^{-5} P$ below-cloud	$2.8 \times 10^{-5} P$ below-cloud $2.8 \times 10^{-5} P$ for cloud SO_4
6	7.4×10^{-6} in summer 4.7×10^{-6} in spring/autumn 1.8×10^{-6} in winter 5.6×10^{-6} rainout	$3.9 \times 10^{-5} P^{0.12}$ in summer $1.0 \times 10^{-5} P^{0.53}$ in spring/autumn $2.5 \times 10^{-6} P^{0.7}$ in winter	$1.1 \times 10^{-4} P^{0.06}$ in summer $2.5 \times 10^{-5} P^{0.27}$ in spring/autumn $5.8 \times 10^{-6} P^{0.7}$ in winter $3.3 \times 10^{-5} P$ for cloud SO_4

[a] Models 5, 7, and 8 used the same parameters as presented in Table 2.

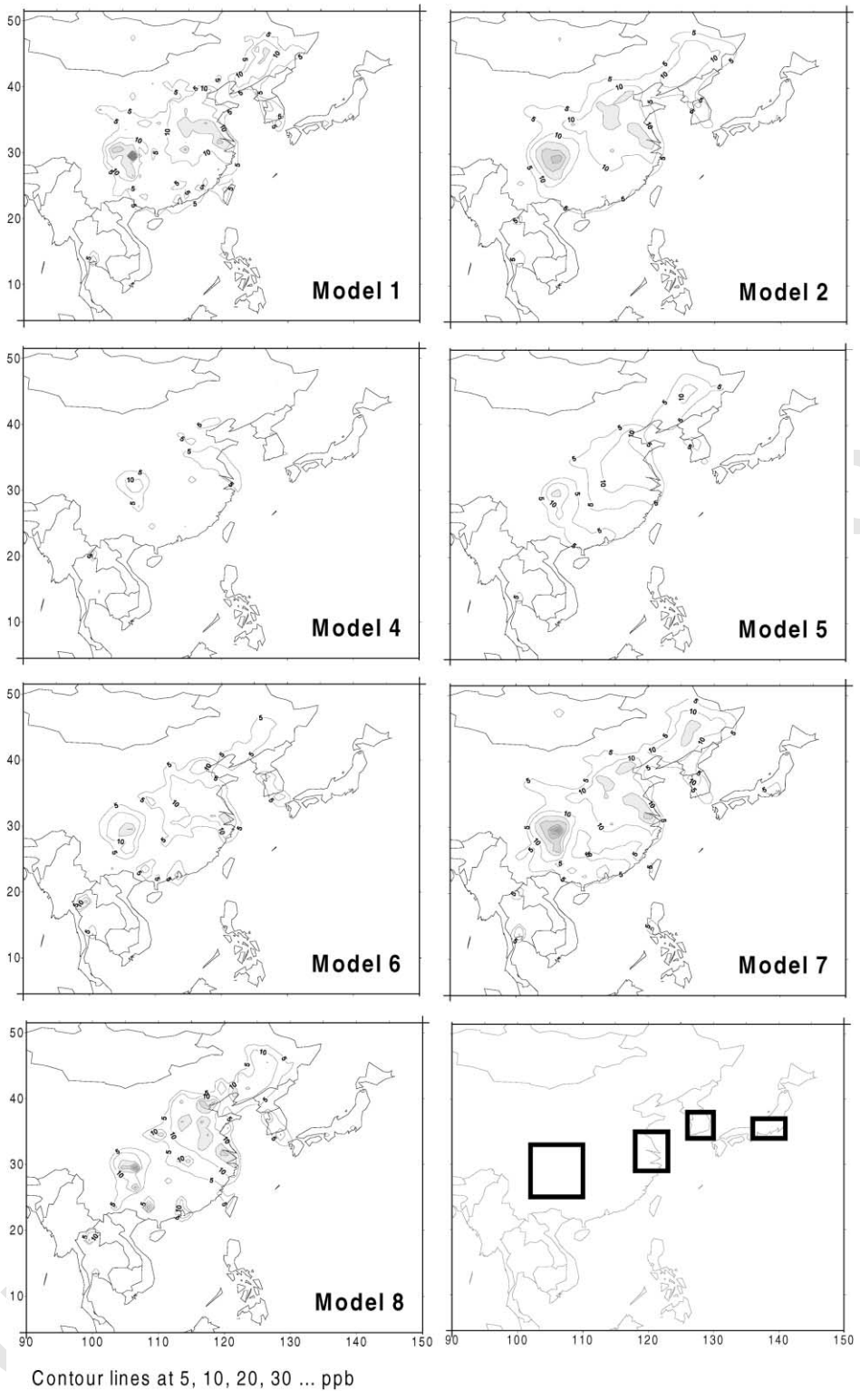

Fig. 4. Example of 10 day-averaged surface SO_2 concentrations (1–10 January) calculated by the participating models. (Task A) Also shown (lower-right panel) are the four regions on which the comparison among models is focused: Central Japan, southern Korea, eastern China and Central China.

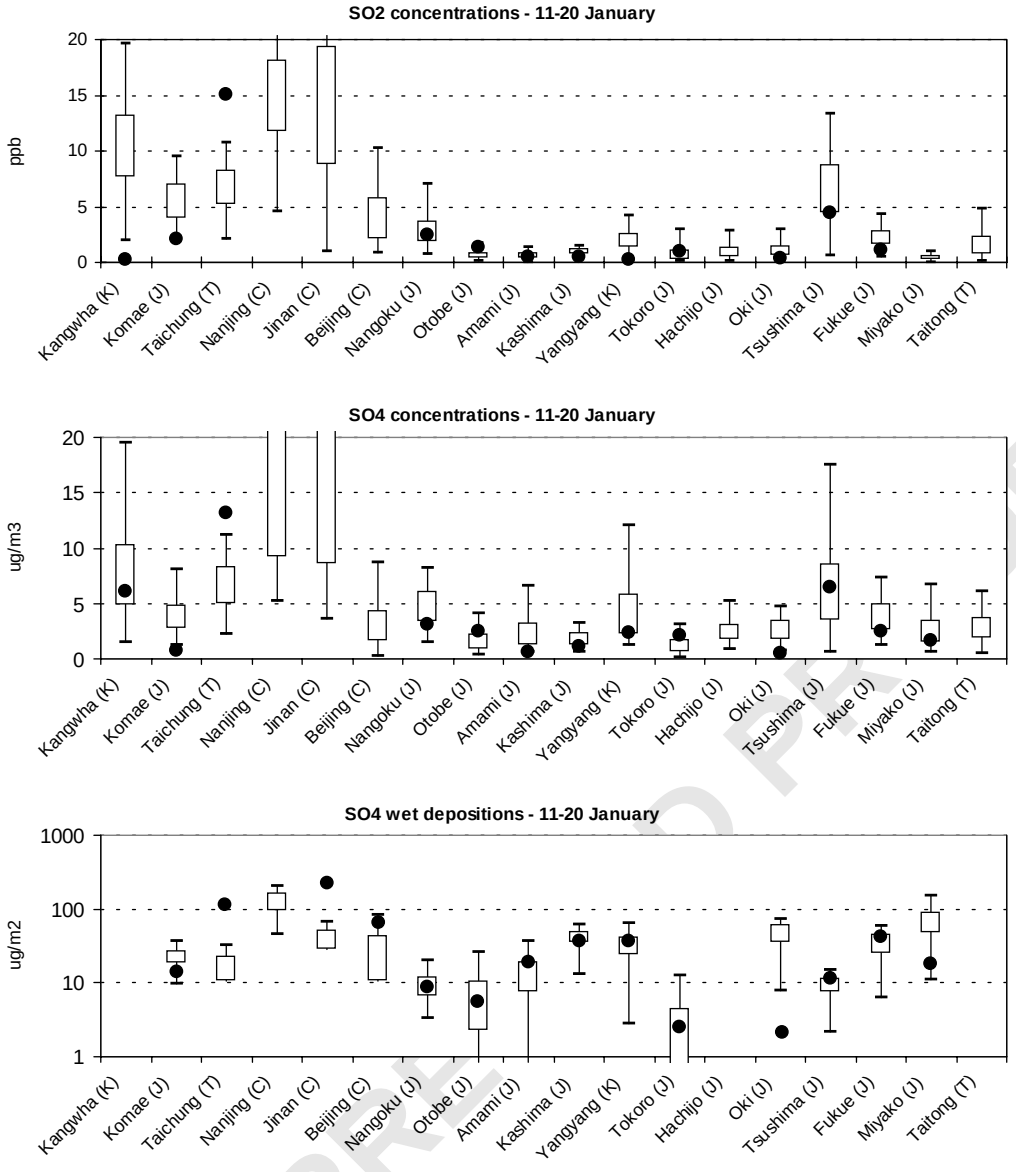

Fig. 5. Comparison with monitoring data for the 11–20 January period. Measurements are represented by dots, while model results are presented as whiskers indicating the distribution of values predicted by individual models (Task A).

performance problems are not seen at nearby sites, suggesting that reasons may be related to horizontal resolution issues, and these were not addressed in this phase of the study.

There are many factors that influence the model results. One very important factor is the direct relationship between sulfate wet deposition and precipitation rate and amount. The analysis of model predicted precipitation against observed amounts (see Fig. 3) showed that the largest underpredictions by the models occurred for cases where the modeled precipitation was underpredicted, and these occurred mostly over the island stations. For this reason measured precipitation amounts were used to adjust modeled wet depositions before the comparison with observations (and through this, model predicted values were found to follow more closely with observations). Furthermore, model performance was found to increase when the comparisons were made on longer time periods (e.g. on a monthly basis; not shown), as a result of the fact that the monthly time frame captured and summed the influence of more precipitation events.

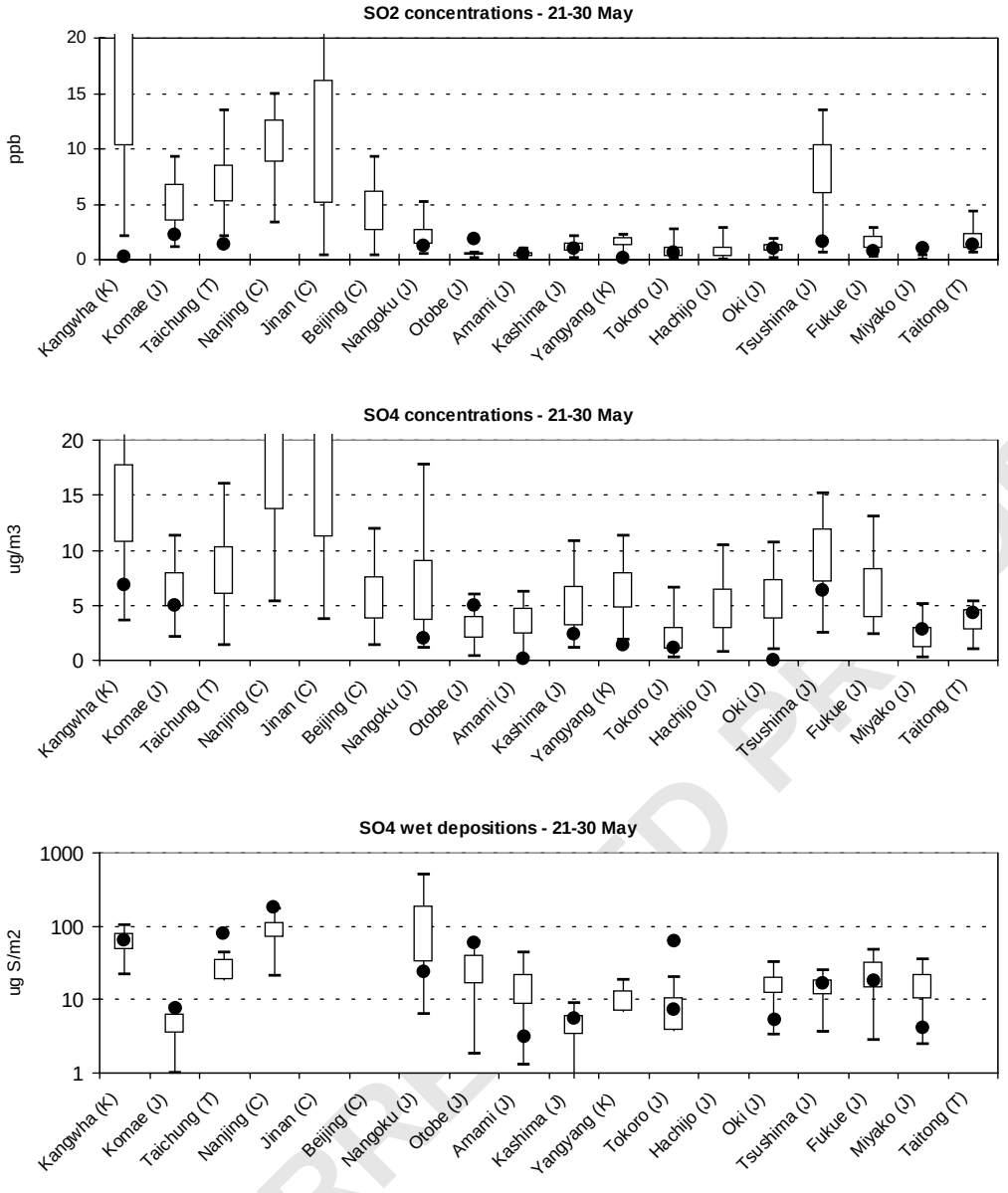

Fig. 6. As in Fig. 5, but for 21–30 May.

4.2. Transport and diffusion

Each model differs in important ways including the numerical algorithm used, model framework, and the vertical resolution (see Tables 5 and 6). Each of these features impacts the resulting calculated spatial and temporal distributions of sulfur concentrations and deposition. To illustrate this point calculated daily mean SO_2 concentrations for 30 May are presented in Figs. 9a and b for two regions: South Korea and southern China (see Fig. 4 for the region locations). The daily mean near-surface concentrations and the boundary layer (0–1 km) averaged distributions computed by all models with fixed parameters (Task B) are shown. All models show the same general features, with the high emission areas clearly located within the subdomains. However the models do differ in terms of the magnitudes of the peak values, and the structure of the horizontal and vertical distributions. For example, in southern Korea, Model 1 shows much stronger horizontal and weaker vertical gradients than Model 5. Models 1 and 8, followed by 2 and 7, also present in general the highest surface maximum (see also Fig. 10).

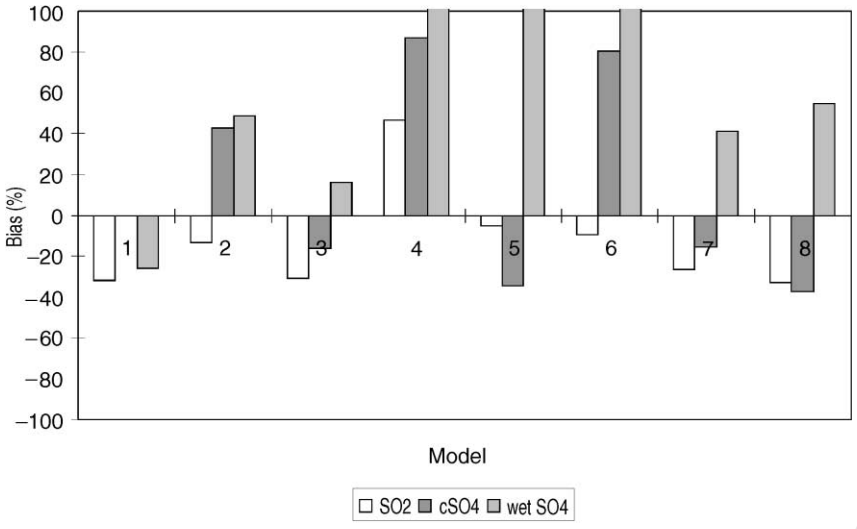

Fig. 7. Bias (as [obs.−calc.]/calc. × 100) of model calculated quantities for the month of January (Task A).

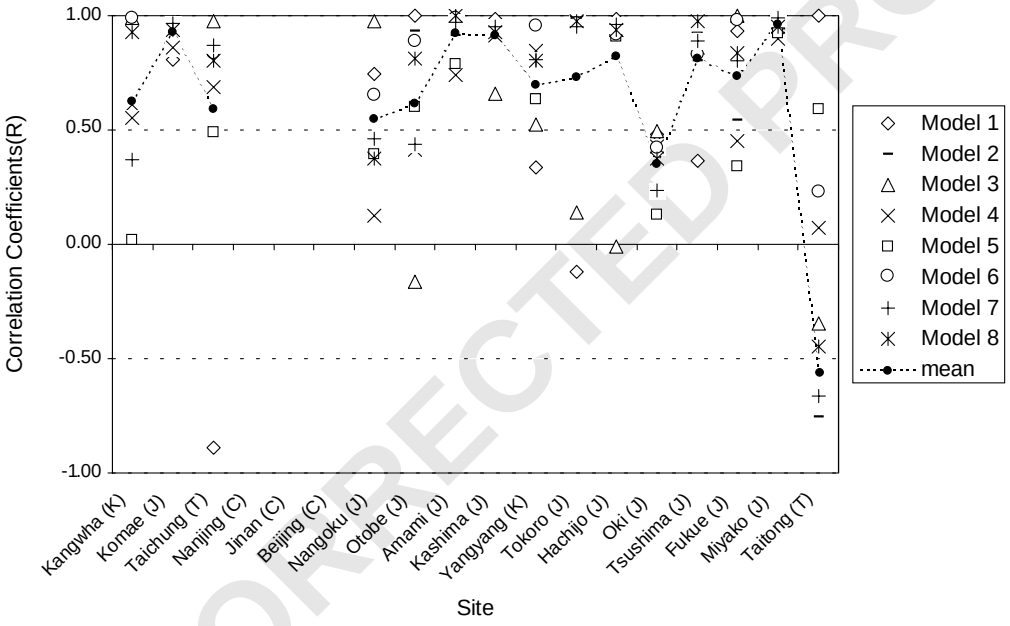

Fig. 8. Correlation between observed and predicted data by monitoring site (Task A).

The differences between model predictions are more clearly depicted in Fig. 11, where the ratio of predicted near-surface to boundary-layer concentrations at various locations are presented. Again the general behavior of all the models is similar, with all models resolving strong vertical gradients in the high source areas such as Komae and Nanjing, and small gradients over island locations with no appreciable anthropogenic SO_2 emissions (e.g., Oki, Amami, Miyako). The only point with boundary layer concentrations higher than surface is at Hachijo, a location heavily impacted by an elevated strong volcanic emission. However the magnitudes of this ratio varies by as much as a factor of 5. Consistent with what was already pointed out for concentrations integrals, Models 2 and 7 generally have higher surface/boundary layer concentration ratios, meaning that they exhibit sharper vertical gradients, while the opposite holds for Model 1, which generally shows a relatively

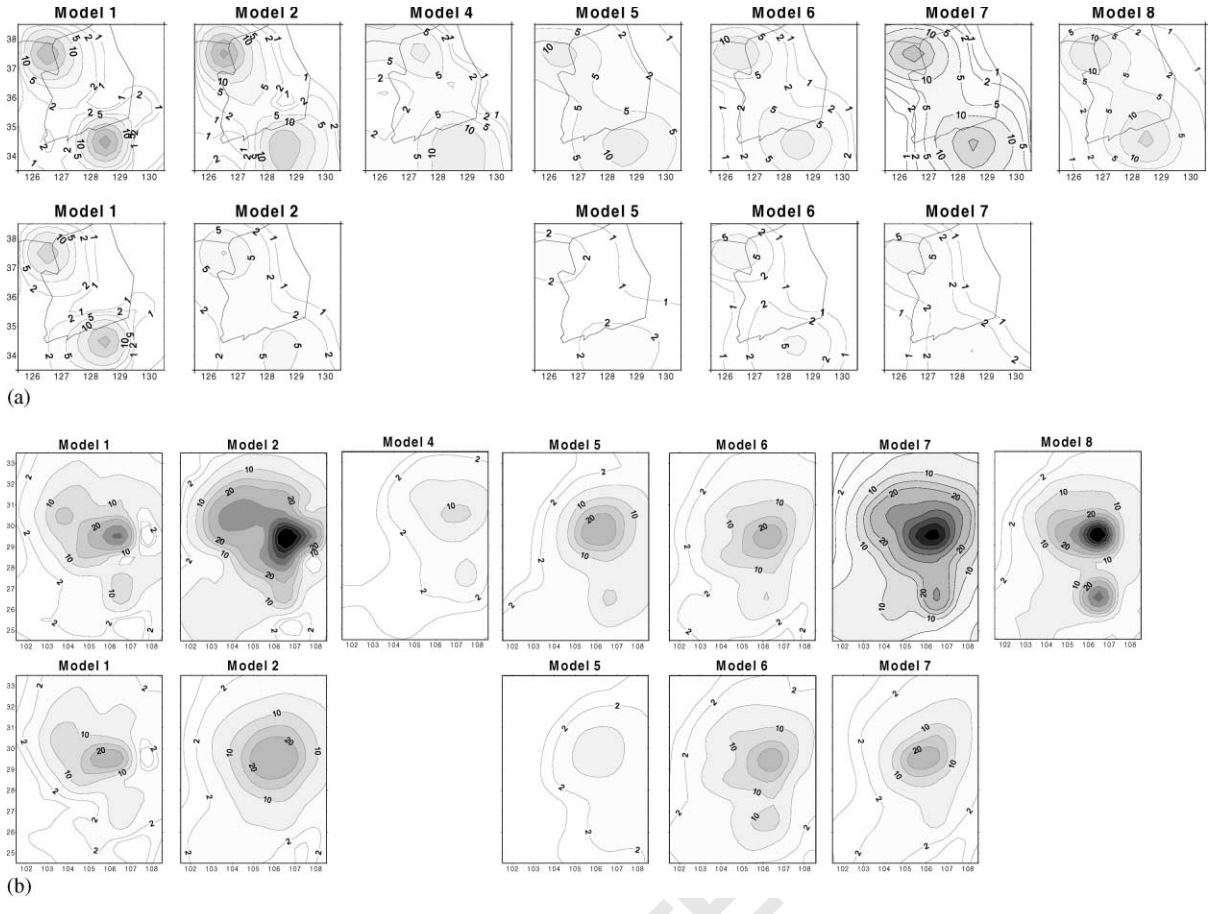

Fig. 9. (a) SO_2 daily surface (top row) and boundary layer averaged concentrations (bottom row) on 30 May over southern Korea (contours at 1, 2, 5, 10, 20, 30, 40… ppb). Note that Model 3 is receptor oriented model and did not produce 2D fields, Models 4 and 8 are 1-layer models so boundary layer averaged plots (not shown) are the same as the surface layer plots. (b) Same as (a), but for Central China (contours at 1, 2, 5, 10, 15, 20, 30, 40… ppb).

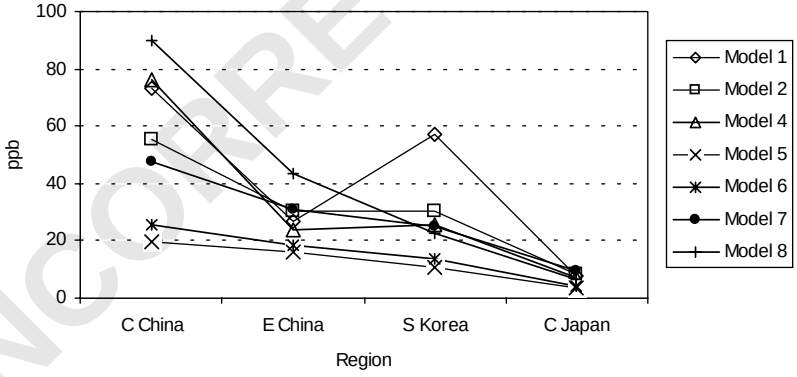

Fig. 10. Maximum surface SO_2 concentrations over regions (21–30 May).

modest vertical gradient in the lower part of the troposphere.

This point is amplified further in Fig. 12, where the masses of SO_2 as sulfur in the lowest 1 km for each of the target regions are presented. Again all models show the same general features in terms of which region has the highest mass loadings (i.e., Central China), but the magnitude of the mass can vary by a factor of 5.

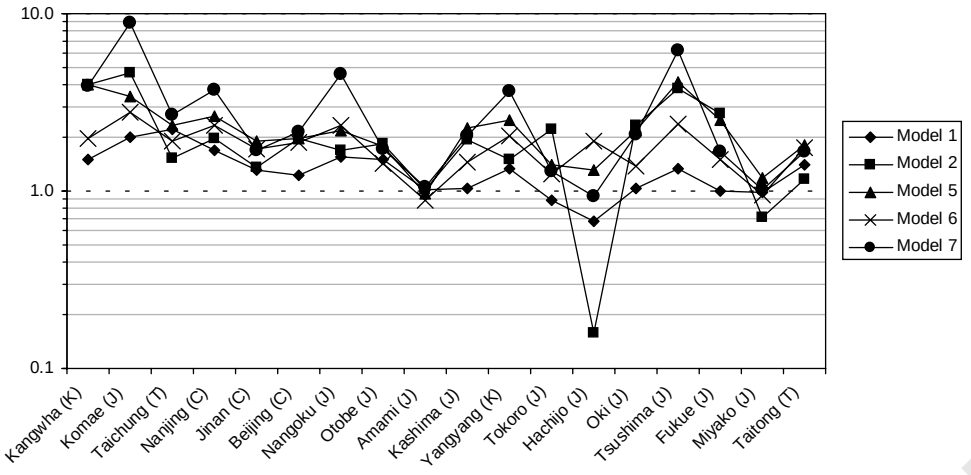

Fig. 11. SO_2 daily concentrations at monitoring stations (30 May): ratio between surface values and the average over the first 1000 m.

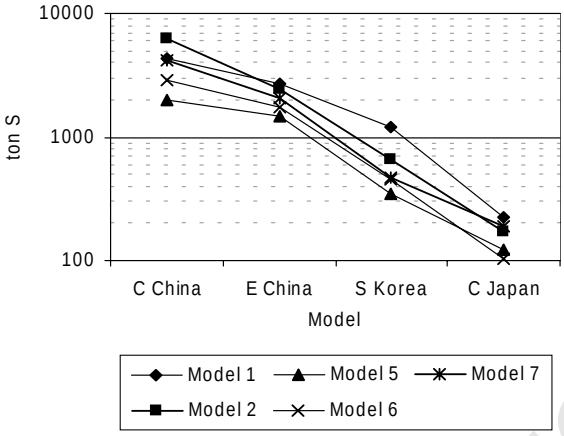

Fig. 12. Integrals in the first 1000 m of SO_2 daily concentrations over the four target regions (30 May).

Similar findings hold for January results as well (not shown). Such differences are less dependent on model framework (Lagrangian vs. Eulerian), than on the number of vertical model layers, and the numerical algorithms (i.e., diffusive characteristics) and assumptions (e.g., whether horizontal diffusion was included explicitly or not) used for horizontal and vertical transport.

4.3. Chemical conversion

The conversion rate of SO_2 to sulfate is a key parameter in determining the partitioning of sulfur between SO_2 and sulfate, and in turn, in determining the pathways for deposition (in what form and by what process—wet/dry), and the overall lifetime of sulfur in the atmosphere. One metric that reflects overall conversion rates in the context of all removal processes is the fraction of sulfur in ambient air present in the form of sulfate. A plot of observed and modeled predicted fraction of sulfur as sulfate in ambient air ($[SO_4]/([SO_2]+[SO_4])$, both species as S) is presented in Figs. 13a and b. Shown are the values calculated by models using their own parameters (Task A). The low value at Amami in May is the result of measurement error with ambient values at/or below the instrument detection limit. These results show that the fraction of sulfur as sulfate is in the range of 0.3–0.4 over Japan, and increases to 0.6–0.8 over China and Korea. The model predicted values are generally consistent with the observations and exhibit higher (or lower) ratios in both months over the same regions.

One interesting feature is that the observations in general do not show a dramatic increase in the fraction as sulfate in May relative to that in January. Based simply on chemical conversion rates, one would expect a marked difference (with the fraction as sulfate in May higher than that in January) as the gas phase conversion rates are about three times higher in May than January. The fact that a large increase is not apparent demonstrates the tight coupling between chemical conversion and transport and removal processes. If the transport and removal characteristics were identical, then based on chemical conversion considerations only, May values of sulfate concentration and sulfate fraction should be higher than those in January, while SO_2 concentrations in January should be higher than those in May. As also shown in Figs. 13c and d there is no clear trend in SO_2 and sulfate levels between May and January. This suggests that the transport and removal characteristics of the events may be different and that they play an unimportant role. The monthly mean wind speeds and

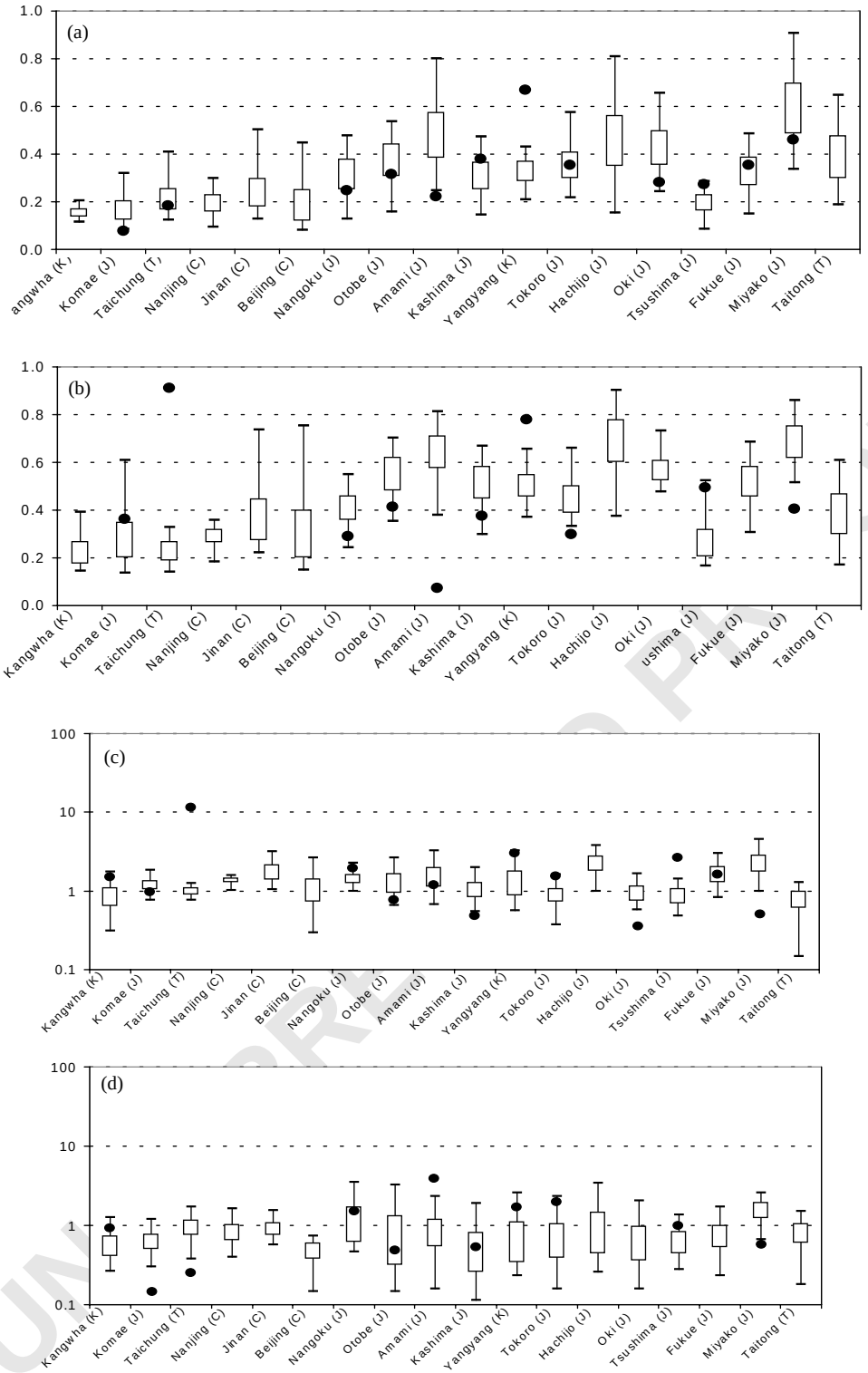

Fig. 13. Fraction of SO_4 in air concentrations: (a) 11–20 January; (b) 21–30 May. January/May ratio calculated for 10 days average concentrations: (c) SO_2; (d) SO_4 (Task A).

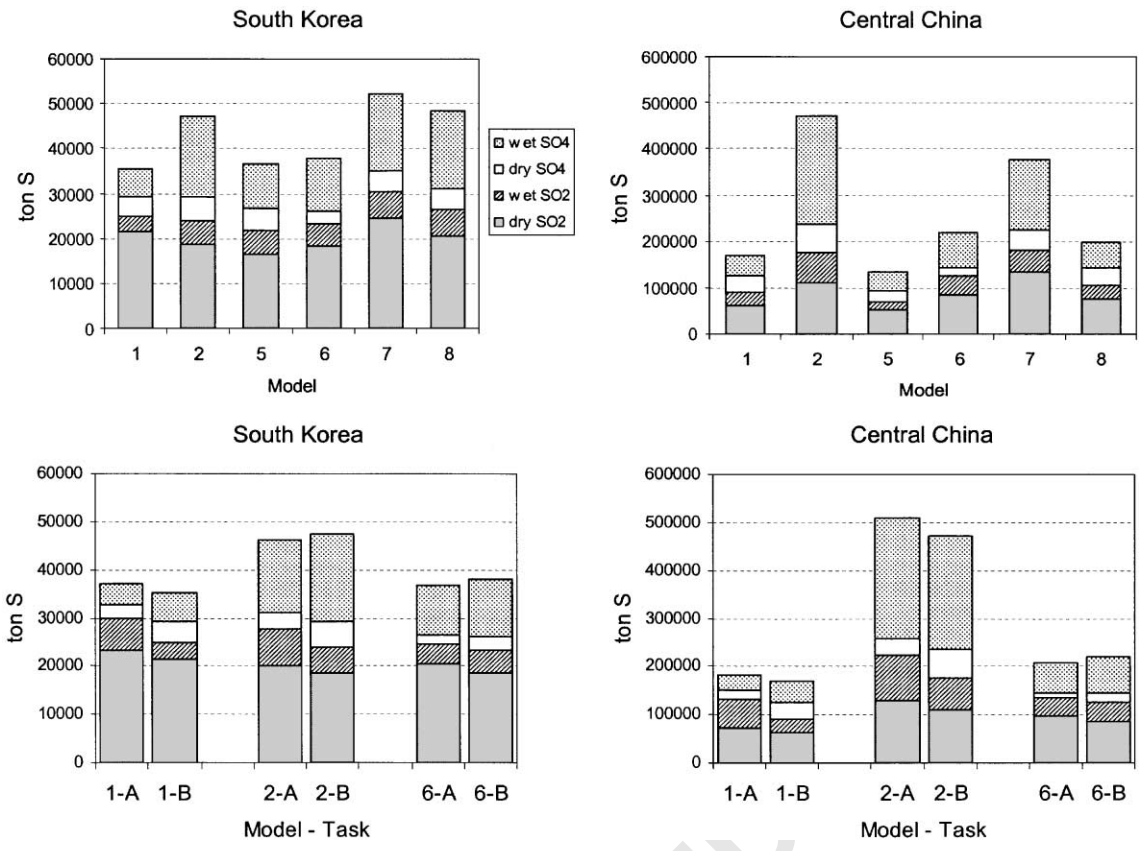

Fig. 14. Total sulfur depositions for both months (January and May together) and contributions due to each process over selected target regions. Upper panels: results from Task B. Lower panels: Task A vs. Task B.

precipitation (Fig. 2) show that the transport speeds and general precipitation patterns are quite similar for these two periods over most of the domain. However, in the case of precipitation the number of events was greater in January, while the intensities were higher in May. Furthermore the precipitation amounts over the high sulfur source regions in eastern China were higher in May. The combinations of these factors control the net sulfate to sulfur ratio.

4.4. Sulfur deposition

The model calculated sulfur deposition was further studied by comparing the sulfur deposition quantities and the contributions due to each process (i.e., dry/wet as SO_2 and sulfate) at the four target regions. Examples of the results compiled for the 2-month period (January and May together) are shown in the upper panels of Fig. 14, for South Korea and Central China. While variations in predicted sulfur deposition range from ~50% in South Korea to 400% in Central China, the predictions are very similar in terms of the relative importance of the various pathways. Dry deposition as

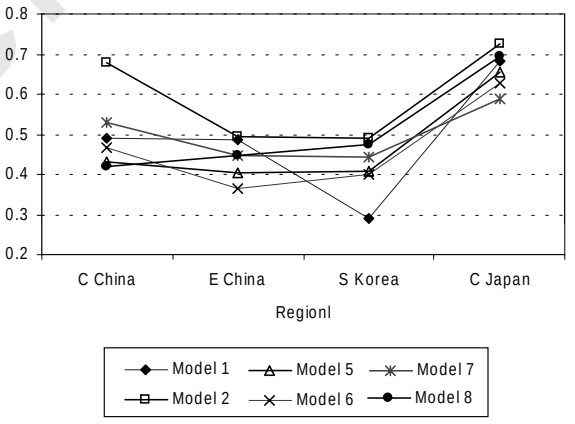

Fig. 15. Wet to total sulfur ratio in depositions for both months (January and May together) over the target regions (Task A).

SO_2 and wet deposition as sulfate are the two dominant terms. In fact the models are very robust in predicting the wet to total sulfur deposition ratio. This is shown in Fig. 15, where all the models predict that the fraction

wet removed over Japan to be between 0.6 and 0.7 and to drop to between 0.35 and 0.5 over eastern China. The predictions of absolute quantities can vary greatly as shown over Central China. Here the differences also show up in the various terms, with Model 2 showing a large wet sulfate contribution (this model also has high sulfate gas phase concentrations). The increased difference among models over Central China may be attributed to the combination of high emission fluxes and low ventilation (see Fig. 2).

It is interesting to assess whether these differences are due to model structure or to differences in the chemical conversion and wet removal parameters. A comparison of model results for Tasks A and B allow a direct evaluation of how much of these differences can be attributed to the chemical and removal parameters used in the model calculations. These results are shown in the lower panels of Fig. 14 for the models that performed both tasks, using different parameters while the parameters used are summarized in Table 7. Relative to the fixed parameter case the SO_2 to sulfate conversion rates varied from 0% to −100%, while the wet removal rates varied by factors of −10 to +2. Quite surprisingly, the results from Tasks A and B are very consistent, indicating that the choice of parameters within this range of values has a remarkably *small* impact on the results, and that the biggest influence is in terms of model structure.

Another key issue in analyzing model performance in comparison with observations is the issue of horizontal resolution. Long-range transport models calculate concentrations and deposition amounts relative to a horizontal grid, while a measurement site obtains values at a fixed point. This fact gives rise to the classical problem of how representative is a point measurement to the value within a model grid cell, and how to take into account this sub-grid scale variability in model analysis. This point is illustrated in Fig. 16, where the measurements sites of Kanghwa and Tsushima are located on SO_2 emissions with resolutions of 1° and 30 s. Kwanghwa and Tsushima when placed within the 1° emissions grid represent sites located within the highest

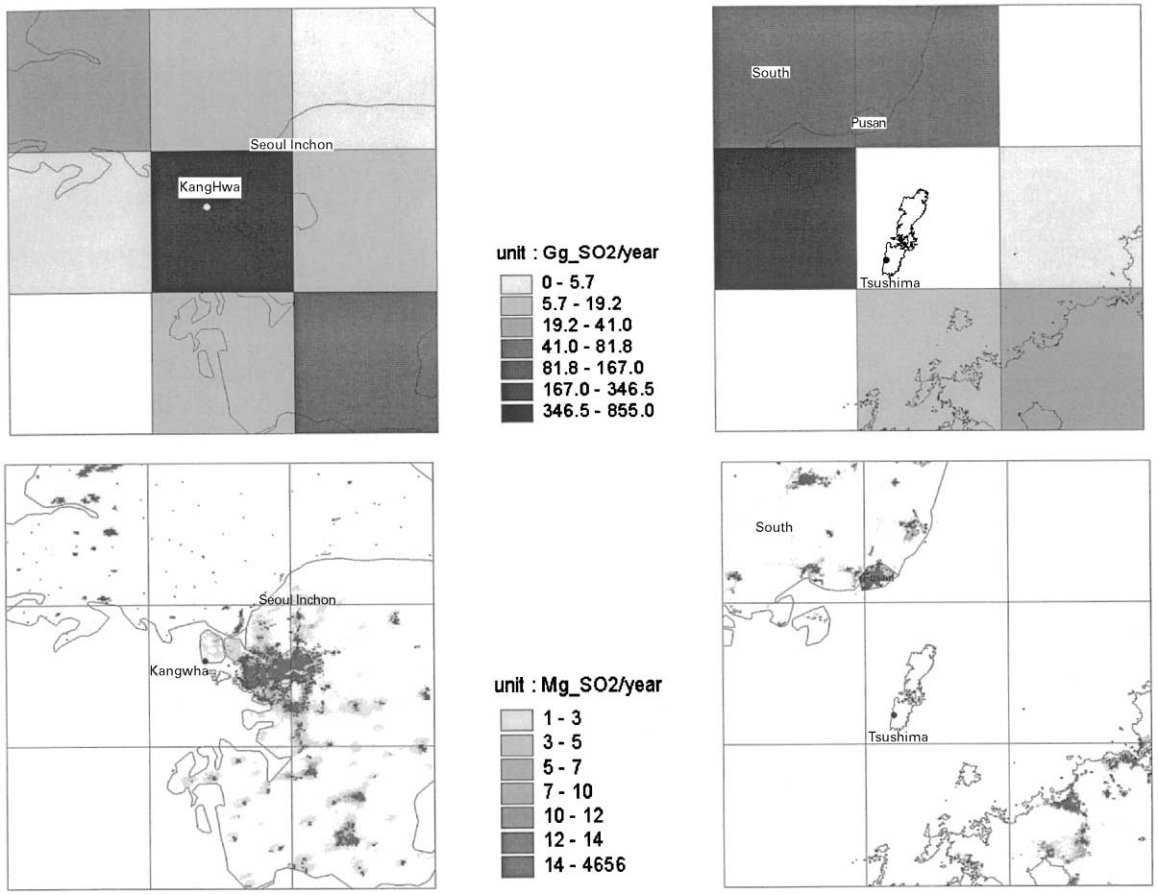

Fig. 16. Monitoring station location and emission distribution at Kanghwa (left) and Tsushima (right); spatial resolution is 1° on upper row and 30 s on bottom row.

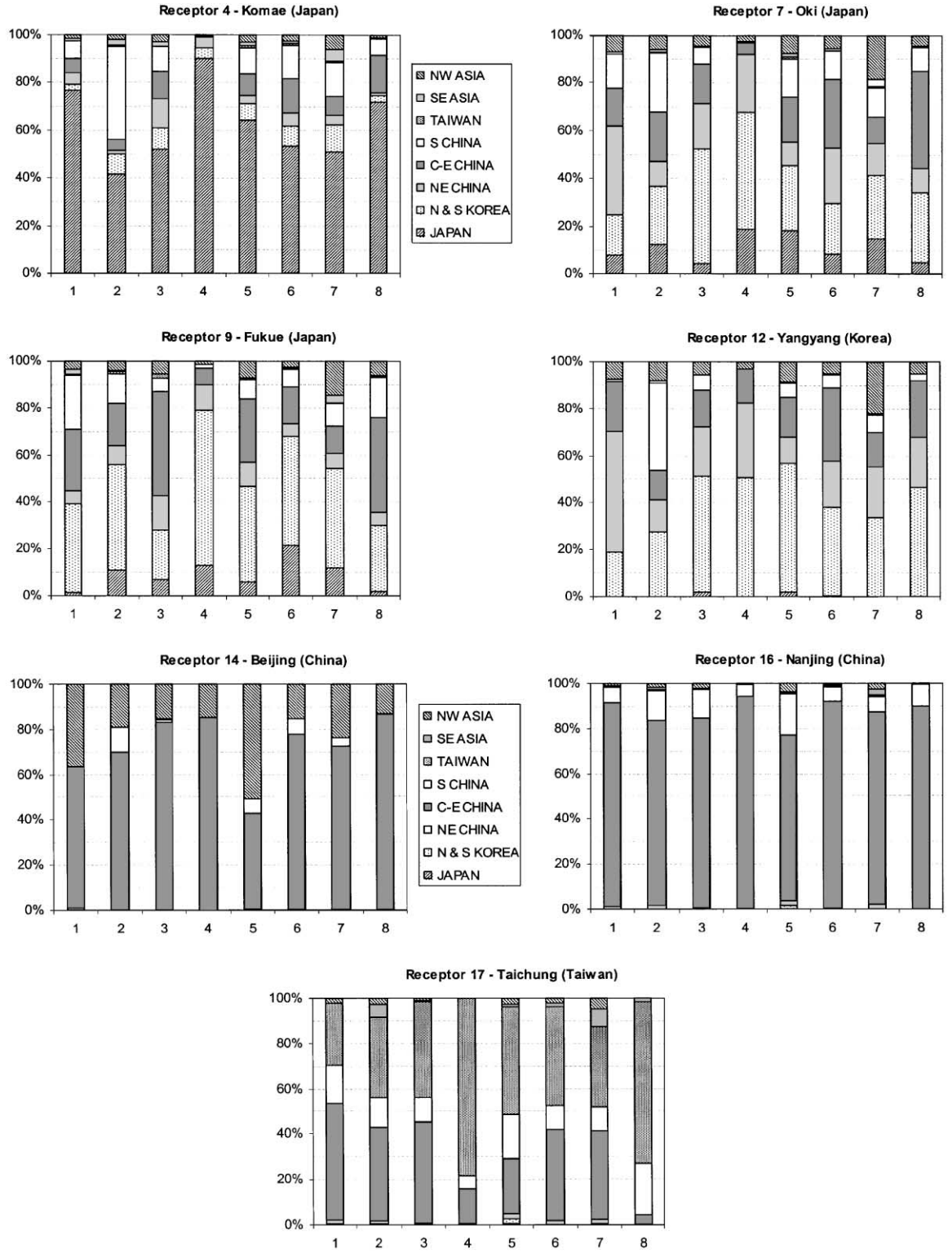

Fig. 17. Source–receptor relationships (anthropogenic sources)—January (Task B).

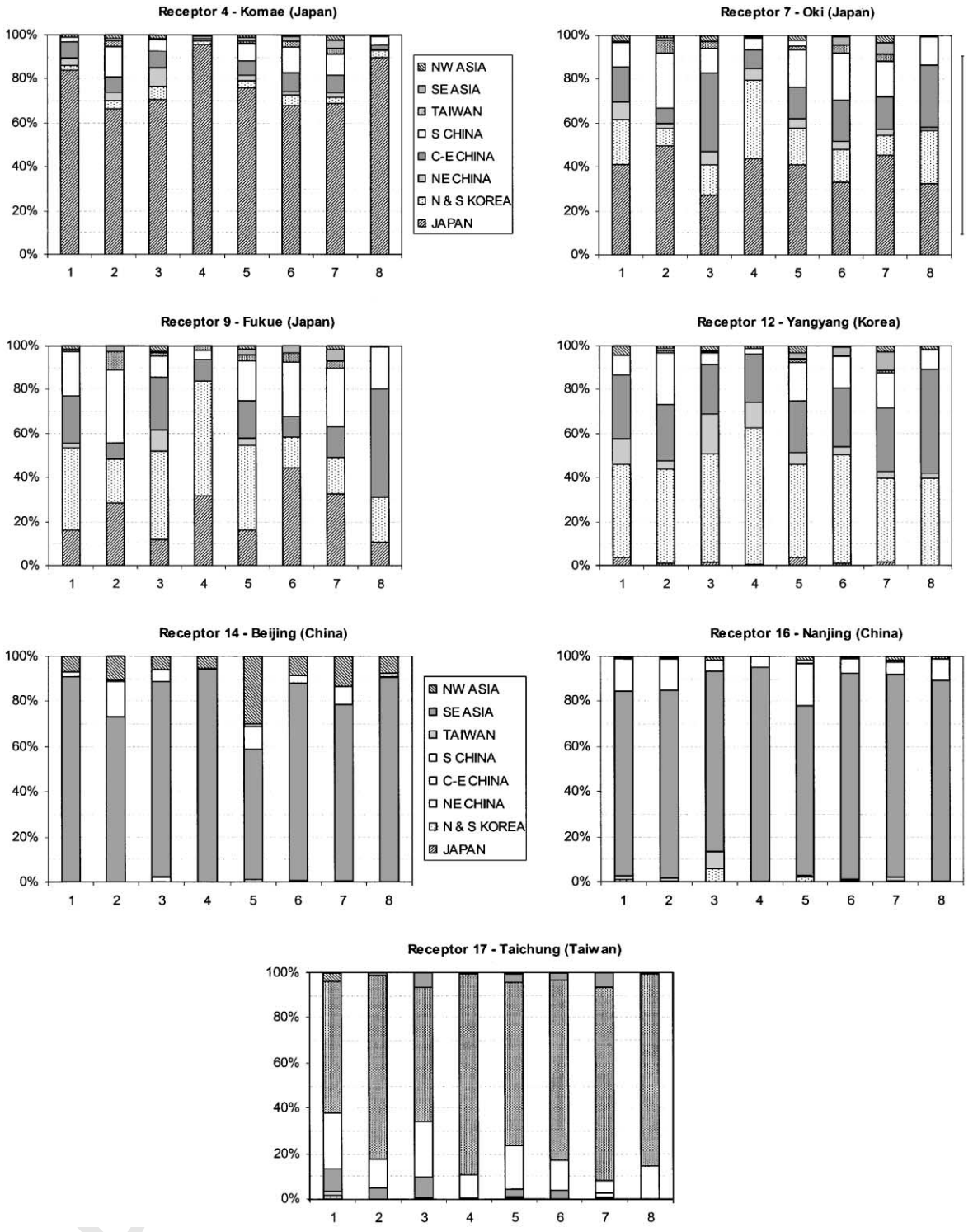

Fig. 18. Source–receptor relationships (anthropogenic sources)—May (Task B).

and 4th lowest emissions, respectively. The models consistently over-predicted the concentrations (both sulfur dioxide and sulfate) at these two sites (e.g., see May values), but do better with sulfur wet deposition. These features can be understood from Fig. 16, where Tsushima is shown to be isolated from local sources for all flow directions, and Kanghwa is isolated from local sources for all flow directions except easterly. Sulfate wet deposition is a more integrated quantity than surface concentrations, and is more heavily influenced by long-range transport, and more reflective of larger scale features. Engardt (2001) in the course of this study explored various ways of interpolating model results to estimate values at specific monitoring site locations. Bi-linear interpolation from surrounding nearest neighbor grid points to the observation site location was found to improve model performance compared to simply reporting the value in the grid where the measurement site is located.

4.5. Source–receptor relationships

To evaluate how model formulation and choice of parameters affect the source–receptor relationships, MICS participants were asked to provide source–receptor relationships at a subset of locations for the set of source regions, shown in Fig. 1. The results are presented in Figs. 17 and 18 for January and May, respectively.

The models show in many instances a remarkable consistency in terms of identifying the major source contributor. For example at Komae in January all models show the contribution from Japan sources to be the greatest single contributor with contributions ranging from 40% to 60%. In both months the contribution of Central eastern China at Beijing is above 60%, and in Nanjing above 80%. Nearby sources are also the greatest contributors to depositions at Yangyang and Taichung, especially in May, with contributions ranging, respectively, from 40% to 60% and from 60% to 90%.

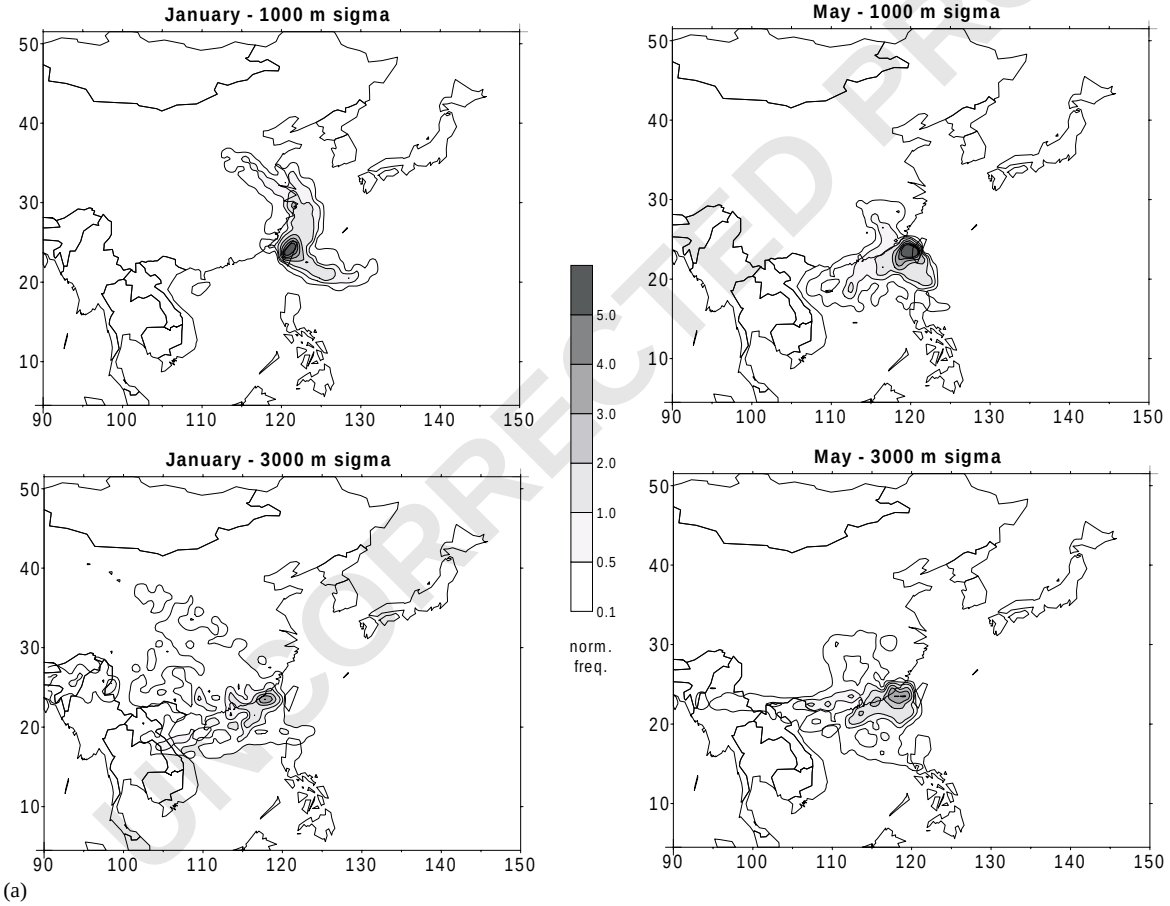

Fig. 19. (a) 5 day iso-sigma back-trajectories arriving in Taichung. Shown are the frequency distribution of all 3-h end points over the entire month of trajectories originated at the receptor. (b) As in (a), but for Fukue.

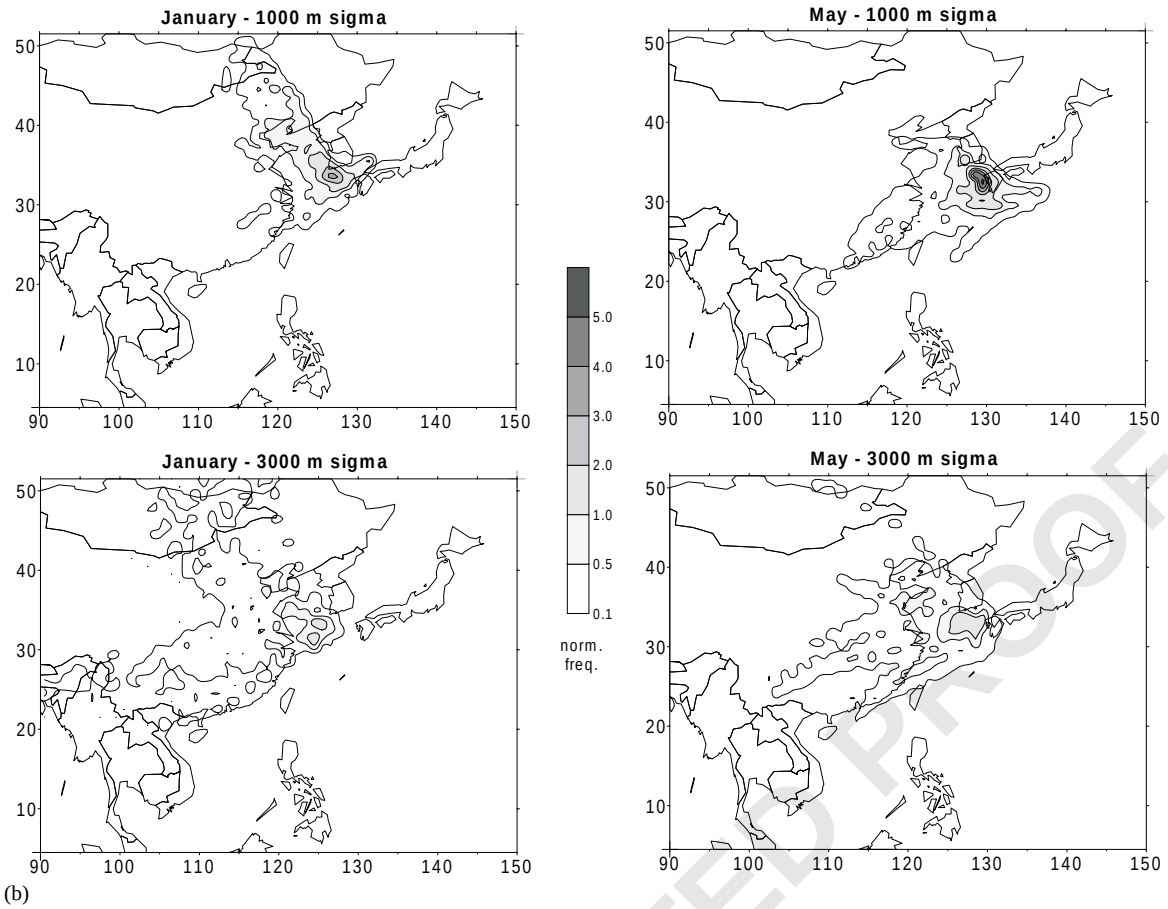

(b)

Fig. 19. (b) (*Continued*)

Noticeable differences do arise; for example the variation in the contribution due to Central eastern China to the receptor at Taichung, and the great structure in contributions to the deposition at Fukue in May. Based on the discussions in Section 4.4, these differences are likely due to transport and vertical resolution issues and not choices of the chemical and deposition parameters. To test this hypothesis statistics of back trajectories were calculated for each receptor and the impact region identified. Trajectories were initiated every 3 h and followed for 5 days. The probability distribution was constructed using all 3-h end-point locations for the entire month. Thus the highest probabilities are near the receptor. Moving away from the receptor reflects going farther back in time. Figs. 19a and b show examples of trajectory statistics at different levels for two of the receptors. The plots for Taichung help explain why the models generally agree in terms of source–receptor relationships in May but differ in January. The effect of the WM on transport (and thus source–receptor relationships) is clearly depicted, with transport in the lower 1 km coming to Taichung either from Central eastern China or from out over the ocean, while the transport above this level originates from the southern China source regions. Variations in the relative contributions of these two sources is the result of transport layers, which in turn depends on model resolution as well as the use of forward or backward trajectories. For May the transport patterns are much less dependent on height. For Fukue the large number of contributing sources and the relative differences are due largely to the fact that this receptor is more centrally located and surrounded by a large number of source regions, and that the trajectories originate from generally wider areas.

4.6. Sensitivity studies

The discussions in this paper have focused on the analysis of results from the participating models for the specific tasks assigned. However, many of the participating modeling groups performed additional studies to better understand how their models performed under the conditions specified. These investigations took the form

of additional systematic studies exploring model sensitivity to the number of vertical layers and the height of the near surface layers, various methods of estimating horizontal and vertical mixing, and different chemical conversion and wet removal rates (Lee and Kim, 2000; Hayami and Ichikawa, 2001; Engardt, 2001). These results indicate that the major factors affecting model performance are the emissions, the driving meteorological conditions, and model formulation factors related to vertical diffusion and mixing height. Vertical resolution was identified as an important factor in diagnosing the depth of the daytime mixed-layer. The sensitivity of the models to these aspects of formulation and parameterization are largest in high emission regions and over land (where diurnal mixing variations are largest), and help explain why the MICS models showed the largest differences over Central China.

5. Concluding remarks

An intercomparison study of long-range transport models in East Asia has been initiated. This exercise has promoted collaborative work in the region and yielded some interesting and important results. For example, the difference in results between Task A and B parameters were found not to differ very substantially in terms of concentrations and depositions, although the chemical conversion and scavenging rates differ by at least a factor of 2. At this stage we judge the uncertainty in emission inventory, and secondarily the driving meteorology, to be much larger than the uncertainty in the model parameters. As the combined results from the different models and tasks have shown, it is in fact difficult to adjust the parameters of these models to cover the broad spectrum of conditions occurring within the domain in different seasons. This problem is also strengthened by the objective difficulties in collecting coherent sets of long-term measurements over the whole area.

Finally, it needs to be emphasized that the main aim of the study was not to rank individual model performances according to their agreement against measurements. Although this is very important, in the current phase of the study attention was rather focused on estimating the uncertainties of predictions made by the set of participating models, and understanding the reasons for the resulting similarities and discrepancies. The results from this study provide an idea about the level of confidence that can be expected from current applications of long-range transport models to East Asia.

Clearly, more work and analysis is needed. The intercomparison study is on going and we invite and encourage others to participate (http://www.cgrer.uiowa.edu/people/gcalori/model_intercomp.htm). There is a plan to expand the focus to include annual deposition and nitrate deposition.

6. Uncited References

Hayami et al., 1999; Ikeda et al., 1997; Uno et al., 1997.

Acknowledgements

This research was supported in part by RAINS-Asia Phase II Project of the World Bank, and by the IIASA-CRIEPI Joint Research Project. Portions of this work were presented at the Acid Rain 2000 meeting in Japan and a brief overview can be found in Carmichael et al. (2001).

References

Arndt, R.L., Carmichael, G.R., 1995. Long-range transport and deposition of sulfur in Asia. Water, Air, and Soil Pollution 85, 2283–2288.

Arndt, R.L., Carmichael, G.R., Roorda, J.M., 1998. Seasonal source–receptor relationships in Asia. Atmospheric Environment 31, 1553–1572.

Bott, A., 1989. A positive definite advection scheme obtained by nonlinear renormalization of the advective fluxes. Monthly Weather Review 117, 1006–1015.

Bott, A., 1992. Monotone flux limitation in the area-preserving flux-form advection algorithm. Monthly Weather Review 120, 2592–2602.

Brost, R.A., Haagenson, P.L., Kuo, Y.-H., 1988. The effect of diffusion on tracer puffs simulated by a regional scale Eulerian model. Journal of Geophysical Research 93 (D3), 2389–2404.

Calori, G., Carmichael, G.R., Streets, D., Thongboonchoo, N., Guttikunda, S.K., 2001. Interannual variability in sulfur deposition in Asia. Journal of Global Environment Engineering, in press.

Carmichael, G.R., Peters, L.K., Saylor, R.D., 1991. The STEM-II regional scale acid deposition and photochemical oxidant model: I. An overview of model development and applications. Atmospheric Environment 25A, 2077–2090.

Carmichael, G., Calori, G., Hayami, H., Uno, I., Yeon Cho, S., Engardt, M., Kim, S.-B., Ichikawa, Y., Ikeda, Y., Woo, J.H., Ueda, H., Amann, M., 2001. A brief overview of the model intercomparison study for long range transport models in East Asia, Water Air and Soil Pollution (Special Issue for Acid Rain 2000), 8.

CGRER, 1999. Model Intercomparison web site. http://www.cgrer.uiowa.edu/people/gcalori/model_intercomp.htm

Christensen, J., 1995. The Danish Eulerian hemisphere model. Proceedings of the 21st NATO/CCMS International Technical Meeting on Air Pollution Modeling and its Applica-

tion, Baltimore, MA. American Meteorological Society, Boston, MA.

Engardt, M., 2001. Sulphur simulations for East Asia using the MATCH model. Water, Air, and Soil Pollution, submitted for publication.

Fujita, S., Takahashi, A., 1994. Acidic deposition in East Asia—design of a cooperative monitoring network for the chemistry of precipitation. CRIEPI Report No. T93091, p. 35 (in Japanese).

Fujita, S., Takahashi, A., Weng, J.-H., Huang, L.-F., Kim, H.-K., Li, C.-K., Huang, F.T.-C., Jeng, F.-T., 2000. Precipitation chemistry in East Asia. Atmospheric Environment 34, 4551–4552.

Guttikunda, S.K., Thongboonchoo, N., Arndt, R.L., Calori, G., Carmichael, G.R., Streets, D.G., 2001. Sulfur deposition in Asia: seasonal behavior and contributions from various energy sectors. Water, Air, and Soil Pollution, in press.

Hayami, H., Ichikawa, Y., 2001. Sensitivity of long-range transport of sulfur compounds to vertical distribution of sources. Water, Air, and Soil Pollution, submitted for publication.

Hayami, H., Fujita, S., Ichikawa, Y., Huang, T.C., Lee, C.K., Jeng, F.T., Chang, J.S., Chang, K.H., Lin, P.L., 1999. Joint Report on Regional Acid Deposition in East Asia. Central Research Institute of Electric Power Industry, Taiwan Power Company, National Taiwan University.

Huang, M., Wang, Z., He, D., Xu, H., Zhou, L., 1995. Modeling studies on sulfur deposition and transport in East Asia. Water, Air, and Soil Pollution 85, 1927–1932.

Ichikawa, Y., Fujita, S., 1995. An analysis of wet deposition of sulfate using a trajectory model for East Asia. Water, Air, and Soil Pollution 85, 1921–1926.

IIASA, 1998. Workshop on Transport of Air Pollutants in Asia, 27–29 July 1998. International Institute for Applied System Analysis, Laxenburg, Austria.

Ikeda, Y., Higashino, H., Ihara, K., Mizohata, A., 1997. The estimation of acid deposition in East Asia. Journal of Japan Society of Air Pollution 32, 116–119.

Lee, T.Y., Kim, S.B., 2000. Comments on "Model Intercomparison Study of Long-Range Transport and Sulfur Deposition in East Asia (MICS-Asia)". Workshop on the Transport of Air Pollutants in Asia (Model Intercomparison Study MICS-Asia), International Institute for Applied System Analysis, Laxenburg, Austria, 18–19 September.

Louis, J.-F., 1979. A parametric model of vertical eddy fluxes in the atmosphere. Boundary-Layer Meteorology 17, 187–202.

Maeda, T., 1998. A comparison of modeled and measured sulfur concentration of precipitation in China. Proceedings of the Sixth International Conference of Atmospheric Sciences and Applications to Air Quality, Beijing, China, November 3–5 (poster presentation).

Matthews, E., 1983. Global vegetation and land use: new high-resolution data bases for climate studies. Journal of Climate and Applied Meteorology 22, 474–487.

Miles, L.M., Yost, K.J., 1982. Quality analysis of USGS precipitation chemistry data for New York. Atmospheric Environment 18, 2889–2898.

Phadnis, M., Carmichael, G.R., 1998. Evaluation of long range transport models for acidic deposition in East Asia. Journal of Applied Meteorology 37, 1127–1142.

Pielke, R.A., Cotton, W.R., Walko, R.L., Tremback, C.J., Lyons, W.A., Grasso, L.D., Nicholls, M.E., Moran, M.D., Wesley, D.A., Lee, T.J., Copeland, J.H., 1992. A comprehensive meteorological modeling system—RAMS. Meteorological and Atmospheric Physics 49, 69–91.

Sellers, P.J., Meeson, B.W., Closs, J., Collatz, J., Corprew, F., Hall, F.G., Kerr, Y., Koster, R., Los, S., Mitchell, K., McManus, J., Myers, D., Sun, K.-J., Try, P., 1995. An overview of the ISLSCP initiative I global data sets. http://daac.gsfc.nasa.gov/CAMPAIGN_DOCS/ISLSCP/OVERVIEW_DOCUMENTS/OVERVIEW.pdf

Robertson, J.K., Wilson, J.W., 1985. Design of the national trends network for monitoring the chemistry of atmospheric precipitation. US Geological Survey Circulation 964, 46.

Robertson, L., Langner, J., Engardt, M., 1999. An Eulerian limited-area atmospheric transport model. Journal of Applied Meteorology 38, 190–210.

Shah, J., Nagpal, T., Johnson, T., Amann, M., Carmichael, G., Foell, W., Green, C., Hettelingh, J.P., Hordijk, L., Li, J., Peng, C., Pu, Y., Ramankutty, R., Streets, D., 2000. Integrated assessment model for acid rain in Asia: policy implications and results of rains-Asia model. Annual Review of Energy and Environment 25, 339–375.

Smolarkiewicz, P.K., 1983. A simple positive definite advection scheme with small implicit diffusion. Monthly Weather Review 111, 479–486.

Streets, D.G., Carmichael, G.R., Amann, M., Arndt, R.L., 1999. Energy consumption and acid deposition in northeast Asia. Ambio 28, 135–143.

Tarrasón, L., 1995. Dispersion of sulphur in the northern hemisphere. A study with a 3-dimensional time-resolved model. Doctoral Thesis, University of Oslo, Norway.

Uno, I., Jang, E.-S., 1999. Outline of RAMS application for model intercomparison dataset. http://www.riam.kyushu-u.ac.jp/taikai/RAMS_RAINS.web/ppframe.htm

Uno, I., Cai, X.-M., Steyn, D.G., Emori, S., 1995. A simple extension of Louis method for rough surface layer modeling. Boundary-Layer Meteorology 76, 395–409.

Uno, I., Ohara, T., Murano, K., 1997. Simulated acidic aerosol long-range transport and deposition over east Asia—role of synoptic scale weather systems. Proceedings of the 22nd NATO/CCMS International Technical Meeting on Air Pollution Modeling and its Application, France, June, pp. 119–126.

Vazquez, J., Perry, K., Kilpatrick, K., 1998. NOAA/NASA AVHRR Oceans Pathfinder Sea Surface Temperature Data Set User's Reference Manual Version 4.0. April, JPL Publication D-14070.